UNIVERSIDAD NACIONAL AUTÓNOMA DE MÉXICO

PROGRAMA DE MAESTRÍA Y DOCTORADO EN INGENIERÍA
ENERGÍA – PROCESOS Y USO EFICIENTE DE LA ENERGÍA.

COMPARATIVE NEUTRONIC ANALYSIS OF THORIUM AND NITRIDE FUELS FOR LEAD-COOLED FAST REACTORS

TESIS
QUE PARA OPTAR POR EL GRADO DE:
DOCTOR EN INGENIERÍA

PRESENTA:

LUIS CARLOS JUÁREZ MARTÍNEZ

TUTOR PRINCIPAL

DR. JUAN LUIS FRANÇOIS LACOUTURE, FI-UNAM

COMITÉ TUTOR

DRA. CECILIA MARTÍN DEL CAMPO MÁRQUEZ, FI-UNAM
DR. GILBERTO ESPINOSA PAREDES, UAM-IZTAPALAPA
DR. EDMUNDO DEL VALLE GALLEGOS, ESFM-IPN
DR. ALEJANDRO NÚÑEZ CARRERA, CNSNS

CIUDAD UNIVERSITARIA, CD. MX., JULIO, 2018

JURADO ASIGNADO:

Presidente: Dr. Gilberto Espinosa Paredes

Secretario: Dra. Cecilia Martín Del Campo Márquez

Vocal: Dr. Juan Luis François Lacouture

1 er. Suplente: Dr. Edmundo Del Valle Gallegos

2 d o. Suplente: Dr. Alejandro Núñez Carrera

Lugar o lugares donde se realizó la tesis: Ciudad de México

TUTOR DE TESIS:

Juan Luis François Lacouture

FIRMA

Acknowledgements

First, I want to express my gratitude to my supervisor, Dr. Juan Luis François Lacouture who has trusted me for this doctoral research, thank you for your patience, knowledge and excellent guidance during my Doctorate studies.

I want to thank to my tutor committee for its constant support during this doctoral project.

To the National Autonomous University of Mexico for giving me the opportunity to pursue postgraduate studies. In addition, for its support with the project PAPIIT-IN115517 and for facilitating the use of the MIZTLI supercomputer under the LANCAD-UNAM-DGTIC-253 project.

To the National Council of Science and Technology (CONACYT), for providing economic support for the accomplishment of this doctoral research.

Abstract

The increasing global energy demand makes it necessary to have alternative energy sources able to fulfill such energy demand as well as reducing the greenhouse gas emissions, whose accumulation would lead to harmful effects for life on the planet. In this research work, the use of nuclear energy is considered as a viable alternative for solving this problem. Nuclear power is an alternative source of energy with low greenhouse gas emissions and high generation capacity for the short, medium and long-term.

Currently, there are several research and development programs related to the new generation of nuclear power reactors that are called to be the future reactors fleet. One of these reactors is the European Lead-cooled Fast Reactor (ELFR), which the main feature is related to its fuel cycle (closed), that allows better use of the resources as well as to reduce the of high-level radioactive waste inventory. The consolidation of this reactor will play an essential role in the European energy framework: therefore, it was selected for this study.

Sustainability, waste minimization and non-proliferation are some of the main objectives of the new generation of nuclear reactors. Therefore, the primary aim of this doctoral research was to develop models based on reactor physics in order to design and analyze the fuel and reactor core of a Lead-cooled Fast Reactor with thorium, studying its breeding and minor actinides transmutation capability.

At first, two thorium fuel configurations were analyzed (homogeneous and heterogeneous). It was found that the best way to use thorium instead uranium is the homogeneous distribution through the core, since Doppler constant, the reactivity effect of coolant density and power distribution were close to those for the reference MOX fuel. Besides, the breeding of ^{233}U would allow an operating cycle greater than 900 days, due to a difference of 1400 pcm of reactivity between the reference MOX fuel and the thorium homogeneous fuel that was found at the end of cycle.

Regarding minor actinides, due to americium is one of the main contributors to spent fuel radiotoxicity, two americium nitride fuel configurations were analyzed (homogeneous and heterogeneous), ranging the Am content in 1, 3, 5, 7 and 9 Wt.%. In addition, some safety parameters were obtained, such as Doppler constant, coolant void worth, and the effective delayed neutron fraction. The highest Am consumption was obtained with the homogeneous fuel configuration: 10.755 kg compared to 1.571 kg for the heterogeneous fuel. Although the homogeneous fuel configuration leads the best Am transmutation rate, the Doppler constant turns positive (660 pcm) with 9 Wt.% of Am, which limits the Am content as much as 7 Wt.% at beginning of cycle for this homogeneous fuel configuration.

Having performed these analyses, it can be concluded that the main goal of this doctoral research was accomplished, since the selected reactor model was successfully validated with the reference literature, and the results indicated that it is possible to extend the reactor operating time with the use of thorium, besides to reducing the minor actinides inventory.

Resumen

La creciente demanda de energía eléctrica mundial hace que sea necesario contar con fuentes alternas de energía capaces de cubrir dicha demanda, y al mismo tiempo reducir la emisión de los gases de efecto invernadero, cuya acumulación daría lugar a efectos adversos para la vida en el planeta. Por lo tanto, en este trabajo de investigación se plantea el uso de la energía nuclear como una alternativa viable para la solución de dicho problema. La energía nuclear es una fuente alterna de energía con una baja emisión de gases de efecto invernadero y una gran capacidad de generación en el corto, mediano y largo plazos.

Actualmente, existen programas de investigación y desarrollo de los reactores nucleares de nueva generación que conformarán la flota de reactores del futuro. Dentro de este tipo de reactores se encuentra el Reactor Europeo Rápido enfriado con Plomo (ELFR), cuya principal característica está relacionada con su ciclo de combustible cerrado, el cual permite una mejor utilización de los recursos, además de la minimización los residuos de alta actividad. La consolidación de este reactor jugará un papel importante en el marco energético europeo, por lo tanto, fue seleccionado para este estudio.

La sustentabilidad, la minimización de los residuos y la no proliferación forman parte de los objetivos de los reactores de nueva generación. Por lo tanto, el principal objetivo de esta investigación doctoral fue desarrollar modelos basados en física de reactores con el objetivo de diseñar y analizar el combustible y el núcleo de un reactor rápido enfriado con plomo, analizando la capacidad de cría con torio y la transmutación de actínidos menores.

Primero, dos configuraciones de combustible de torio fueron analizadas (homogénea y heterogénea). Se observó que la mejor forma de usar torio, en vez de uranio, es con una distribución homogénea en el núcleo, ya que la constante Doppler, el efecto de la reactividad con la densidad del refrigerante y la distribución de potencia, tuvieron valores cercanos a los del combustible de referencia (MOX). Además, la cría de ^{233}U permitiría un tiempo de operación mayor a 900 días, debido a la diferencia de reactividad (1400 pcm), entre el combustible de referencia MOX y el combustible homogéneo de torio, encontrada al final del ciclo.

Respecto a los actínidos menores, ya que el americio es uno de los principales contribuyentes en la radiotoxicidad del combustible gastado, se analizaron dos configuraciones de combustible de nitruro de americio (homogéneo y heterogéneo), variando el contenido de Am en 1, 3, 5, 7 y 9 Wt. %. Además, se obtuvieron algunos parámetros de seguridad, tales como la constante Doppler, el valor de la fracción de vacíos, y la fracción efectiva de neutrones retardados. El mayor consumo de Am se obtuvo con la configuración homogénea del combustible: 10.755 kg comparado con 1.571 Kg de la configuración de combustible heterogénea. Aunque con la configuración homogénea se obtuvo la mejor tasa de transmutación de Am, la constante Doppler se vuelve positiva (660 pcm) para el 9 Wt.% de Am, lo cual limita el contenido inicial de Am a un máximo de 7 Wt.%, para esta configuración homogénea de combustible. Con estos análisis se puede concluir que se logró el objetivo principal de esta investigación doctoral, ya que el modelo del reactor seleccionado fue validado con éxito con la literatura, además los resultados indicaron que es posible extender el tiempo de operación del reactor con el uso de torio, además de que se puede reducir el inventario de actínidos menores.

Contents

List of figures

List of Tables

Introduction

Nowadays we live in an energy dependent society. This dependency has been growing year by year and is caused mainly by two reasons: the increase in world´s population and the economic development of countries (Saito, 2010).

According to United Nations (UN), the worldwide population was ~7.6 billion people in 2017, and it is expected to reach ~8.600 billion people by the year 2030. This population will still be increasing up to ~9.8 billion by the year 2050 and ~11.6 billion by the year 2100. Consequently, the energy demand will depend mainly on world population, since having a higher number of inhabitants in the world a more considerable amount of energy will be required to meet the daily needs of each person (UN, 2017).

Around 80% of energy production comes from fossil fuels like coal, oil and natural gas. The use of these energy sources leads to the so-called greenhouse gas emissions, being the carbon dioxide (CO_2) the major contributor (Saito, 2010). The accumulation of greenhouse gas emissions in the atmosphere can cause an adverse effect on the environment. The earth´s average temperature can increase producing changes in climate conditions like floods, droughts, heavy rains and more frequent and severe heat waves (IAEA, 2016).

Therefore, it is vital to adopt alternative energy technologies, which allow reducing the adverse impact produced by greenhouse gas emissions and while can fulfill the global energy demand. Nuclear power, as a low carbon technology, becomes an important energy source able to satisfy the global energy demand reducing the environmental impact (IAEA, 2016).

Until April 2017, 449 nuclear power reactors were operating around the world in 30 different countries, whose represent a total installed capacity of 392,499 MWe, providing ~16 % of the global electricity generation. The United States of America is the country with the most significant number of nuclear power reactors (99 units), followed by France with (58 units), and Japan with (42 units). Also, 15 new nuclear power plants were under construction (IAEA, 2017a).

It is estimated that about 2 billion tons of carbon dioxide (CO_2) would be produced annually in the world, additionally to those already generated if nuclear power plants were not included in the global energy production, hence, nuclear energy is emerging as an excellent candidate to produce energy in the near future (IAEA, 2017b).

Since Enrico Fermi achieved the first self-sustained chain reaction in 1942, the design and technology of nuclear power reactors has gradually evolved. The nuclear technology evolution can be classified into four generations (Kim et al., 2014).

Generation I (~1950-1970): First prototype reactors.
Generation II (~1970-2000): Commercial reactors mainly Light Water Reactors (LWR) and Heavy Water Reactors (HWR).
Generation III and III+ (~2000): Evolutionary designs of generation II, more reliable, economical, and safer than the previous generation.
Generation IV (~2030): Innovative designs, cheaper, safer, and more proliferation resistant than any reactor of any previous generation (Kim et al., 2014).

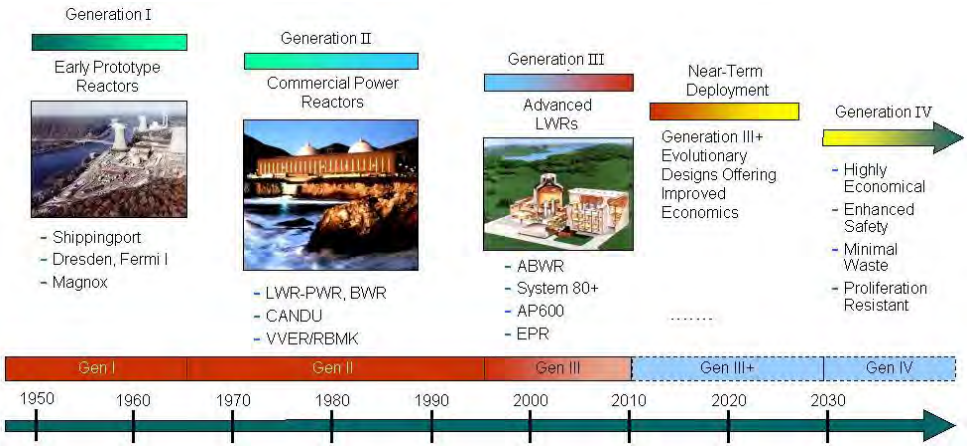

Figure 1. Time line of nuclear reactor technology (Goldberg and Rosner, 2011).

Taking into account the need of a global decarbonisation mainly for electricity generation, in 2002 six reactor technologies were selected to be developed, with the aim of having new power reactors that are safer, cheaper, more sustainable and more proliferation resistant than previous generations. This generation is known as GEN IV power reactors. (GEN IV, 2017a).

Currently, several countries around the world work together on the development of the so-called GEN IV power reactors, and it is expected that they reach a commercial level by the year 2030 (GEN IV, 2017a).

Reactor technologies selected (GEN IV, 2017a):

- Molten Salt Reactor (MSR).
- Supercritical Water-cooled Reactor (SCWR).
- Very High-Temperature Reactor (VHTR).
- Gas-cooled Fast Reactor (GFR).
- Sodium-cooled Fast Reactor (SFR).
- Lead-cooled Fast Reactor (LFR).

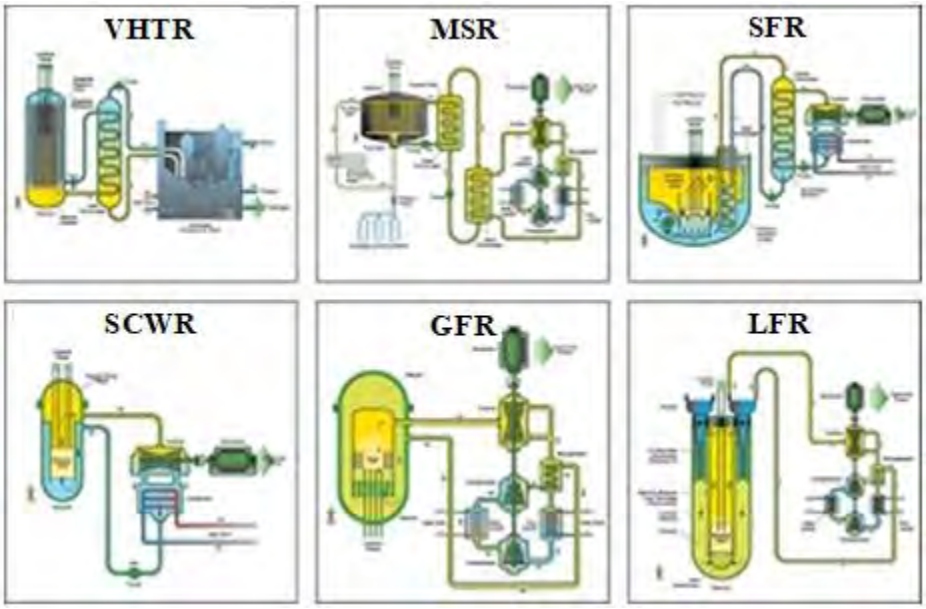

Figure 2. GEN IV power reactors (GEN IV, 2017a).

The reactors mentioned here have some interesting characteristics compared with the previous generations. For example, three of them are fast systems (SFR, GFR and LFR) make them suitable for breeding of fissile fuel or transmute nuclear waste. The majority of them consider a closed fuel cycle (SFR, GFR, LFR and MSR) allowing better use of the resources and reducing the amount of nuclear waste. Finally, some of them could be used for non-electricity applications like hydrogen production and water desalination (Marques, 2010).

Most of the aforementioned reactors use UO_2 and MOX as fuel. Regarding the sustainability goal, it is necessary to have fuel alternatives that allow better use of the resources to extend nuclear energy life. Therefore, thorium being three to four times more abundant than uranium over the Earth's crust becomes an excellent candidate to be used as nuclear fuel. However, due to the lack of fissile content in natural thorium, it is necessary to convert the fertile nuclide ^{232}Th into a fissile nuclide such as ^{233}U. Good options to carry out this process are fast systems, since their high neutron flux that facilitates the transmutation process (Juárez-Martínez and François, 2018).

On the other hand, the spent nuclear fuel contains a mixture of transuranic elements (Pu, Am, Cm, and Np), and they contribute to the long-term spent fuel radiotoxicity. That is why it is necessary to consume these transuranic elements, or convert them into less radioactive elements, and this can be achieved in fast reactors (IAEA, 2009a).

Also, nitride fuels are good candidates for transmutation tasks due to their high density of heavy atoms and their high melting point, which allows operating at higher power densities and longer burn-up levels compared to the conventional UO_2 and MOX fuels (Konings et al., 2012).

One of the six GEN IV reactors selected is the Lead-cooled Fast Reactor. The main feature is related to its coolant, which does not react exothermically with water, as water and sodium do, in addition,

its high melting point (~1743°C) makes the reactor safer and cheaper than other systems (Alemberti et al., 2013; Aufiero et al., 2013).

Taking into account the aforementioned, the primary aim of this doctoral research was to develop models based on reactor physics to design and analyze the fuel and reactor core of a Lead-cooled Fast Reactor with thorium, studying its breeding and minor actinides transmutation capability.

The structure of this thesis is as follows:

- In Chapter I, the main features of LFR technology are presented.
- Chapter II is related to the thermo-physical properties of Lead.
- In Chapter III, the reactor model selected for this doctoral research is presented along with its main characteristics.
- In Chapter IV, a general review on the use of thorium as fuel is given.
- Chapter V is about Minor Actinides (MAs) transmutation characteristics.
- In Chapter VI, the main features of nitrides fuels are presented.
- In Chapter VII, the description of the reactor model selected is given.
- In Chapter VIII, the reactor model validation with Serpent code is presented.
- In Chapter IX, the neutronic study on the use of thorium as fuel is presented.
- In Chapter X, a study related to MAs transmutation with nitride fuel can be found.

Chapter I

Lead-cooled fast reactor (LFR)

The LFR was conceived and designed by the former Soviet Union in the 60s. The main purpose was using these reactors for submarine propulsion, the reason why 12 reactors were designed and operated from 1960 up to 1990, which represents an operational experience about 80 reactor-years (Alemberti et al., 2013).

The LFR has the following features:

- Operates under a fast neutron spectrum (Energy ≥ 0.5 MeV).
- The coolant can be lead or a mixture of Pb-Bi eutectic.
- A closed fuel cycle is expected, which is suitable for minor actinides management.
- The coolant temperature ranges from 420 °C to 560 °C, inlet and outlet temperature, respectively.
- It can be operated as a breeder or as a burner reactor.
- The efficiency is about 44% (Alemberti et al., 2013; GEN IV, 2017b).

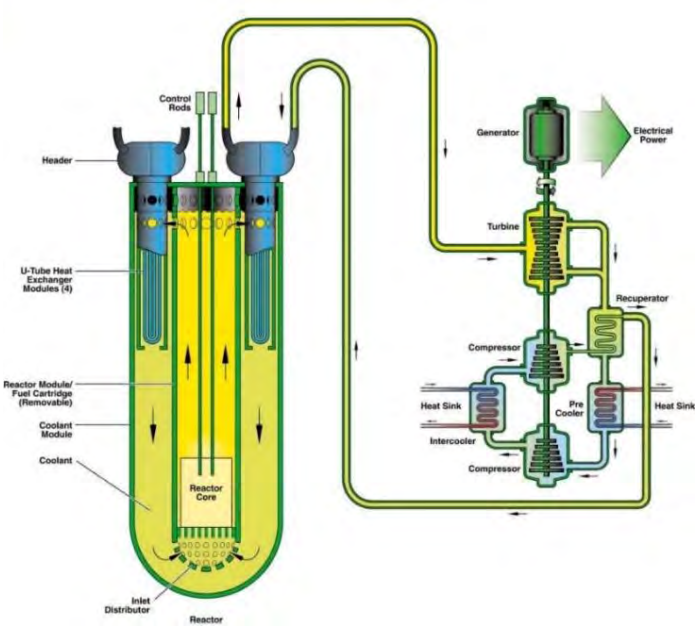

Figure 3. LFR concept (GEN IV, 2017b).

As mentioned before, thanks to no exothermic chemical reaction occurs in contact with air and water, the LFR system has a compact design due to the heat exchangers can be set inside the primary loop, eliminating intermediate heat exchangers as in sodium cooled fast reactors, making the LFR system cheaper with a less capital cost (Zhang, 2012).

In addition, the LFR can operate at low pressure (1 atm) without the risk of core voiding due to coolant boiling, thanks to the high melting point of lead (~1743 °C) (Aufiero et al., 2013; Smith and Cinotti, 2016).

Lead has low neutron moderation, which allows greater spacing between fuel pins, leading to low core pressure loss and reduced risk of flow blockage (Smith and Cinotti, 2016). Compared to sodium reactors, the lead density has a higher decrease for a unit temperature increase which allows a high level of natural cooling circulation in the primary system, see equations 1 and 2 (Zhang, 2012; ENEA, 2016).

$$\rho_{Pb} = 11441 - 1.2675T\ [K] \tag{1}$$

$$\rho_{Pb} = 1012 - 0.2205T - 1.923x10^{-5}T^2 + 5.637x10^{-9}T^3[K] \tag{2}$$

where $\boldsymbol{\rho_{pb}}$ is given in [Kg/m^3].

Another essential feature of lead is that acts as radiation shielding, due to its high-density absorption of gamma rays from nuclear fuel and retaining fission products like Cs and I, which is useful regarding radiological protection (Smith and Cinotti, 2016).

The LFR is intended for electricity generation, hydrogen production, and minor actinides transmutation. However, it requires significant advances in fuels, material performance and corrosion control (Alemberti et al., 2013). Corrosion is considered the main drawback in LFR systems, making that coolant velocity must be kept below 2 m/s to avoid the erosion of cladding and structural materials, which limits the fuel temperature and heat removal (Aufiero et al., 2013).

Russia, USA, Eastern Europe and some Asian countries, like Korea, Japan and China, are the countries with the most significant progress in the LFR development. They have already developed some reactor concepts, as is shown next along with their main features (Alemberti et al., 2013).

1.1. Main LFR prototypes

1.1.1. Small Secure Transportable Autonomous Reactor (SSTAR)

The SSTAR is a modular fast reactor designed by the USA, which can provide about 20-45 MWe. Its main features are presented next (Smith et al., 2008):

- Nitride fuel with transuranic elements.
- Pb as a coolant with a mass flow of 2150 Kg/s.
- Inlet and outlet coolant temperature: 420/564 °C.
- Maximum cladding temperature: 650 °C.
- Active zone height: 0.976 m.
- Active zone diameter: 1.22m.
- Vessel dimensions height/diameter: 12/3.23 m.
- Bryton supercritical CO_2 cycle with an efficiency of 44.2%.

Fig. 4 shows the reactor configuration.

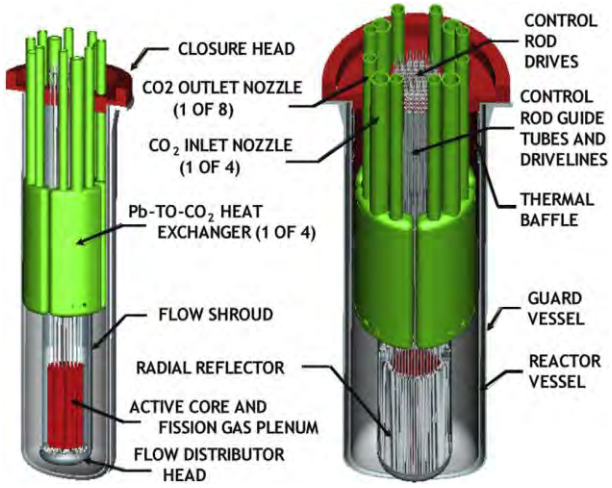

Figure 4. SSTAR reactor (Smith et al., 2008).

1.1.2. The Russian BREST OD-300

The BREST is a 300 MWe demonstrator reactor and is a prototype of the future BREST commercial reactor (Bystry Reaktor Estestennoy Bezopasnosti). The main features are listed below (Alemberti et al., 2013; Glazov et al. 2007):

- Power: 700 MWt, 300 MWe.
- Fuel: (U-Pu-MA)N.
- Coolant: Pb.
- Inlet and outlet coolant temperature: 400/480 °C.
- Maximum coolant velocity: 2 m/s.
- Core height: 1.1 m.
- Core diameter: 2.6 m.
- Maximum cladding temperature: 650 °C.
- Total Efficiency: 43-44%.
- Core breeding ratio ~1.

Fig. 5 shows the BREST-OD-300 reactor and the plant configuration.

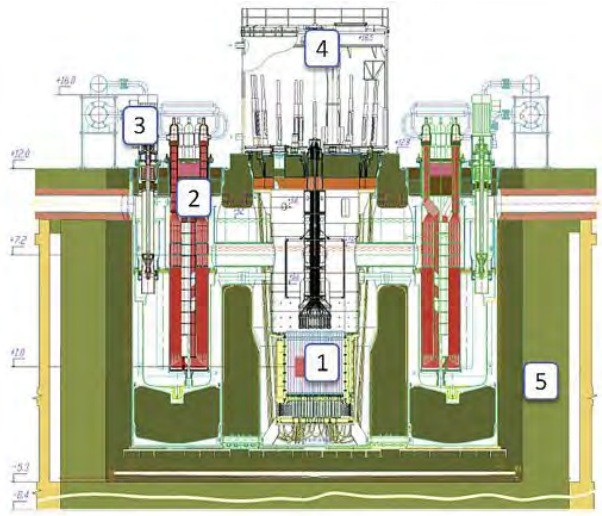

Figure 5. BEST-OD-300 configuration: 1) Reactor Core; 2) Steam Generator; 3) Pump; 4) Reloading machine; 5) Reactor well (Alemberti et al., 2013).

1.1.3. Advanced Lead Fast Reactor European Demonstrator (ALFRED)

Currently, the European Union has financed the project LEADER (Lead-cooled Demonstration European Advanced Reactor) in which they have developed preliminary designs of an industrial size lead-cooled fast reactor (1500 MWth) and its 300 MWth demonstrator reactor called ALFRED (Grasso et al., 2014).

As a demonstrator reactor, ALFRED has the main aim to prove the viability of the European lead-cooled fast reactors and provides technological solutions to accelerate the design and licensing of LFR systems (Grasso et al., 2013a).

The main ALFRED features are shown next (Grasso et al., 2014):

- Power: 300 MWt.
- Fuel: MOX.
- Coolant: Pb.
- Inlet and outlet coolant temperature: 400/480 °C.
- Maximum coolant velocity: 3 m/s.
- Core height: 0.6-0.9 m.
- Maximum diameter: 1.7 m.
- Maximum cladding temperature: 750 °C.
- Fuel assemblies geometry: Hexagonal.

The core layout and reactor configuration are shown in **Fig. 6**.

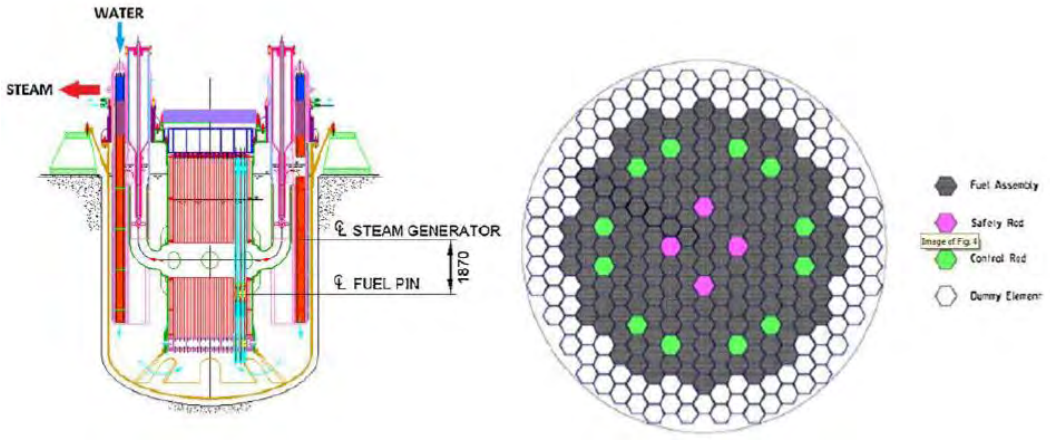

Figure 6. ALFRED configuration and core layout (Grasso et al., 2014).

1.1.4. The European Lead-cooled Fast Reactor (ELFR)

The ELFR is an evolutionary design of the European Lead-cooled System (ELSY). It is a big size reactor designed to provide a power of 600 MWe with an efficiency of 42%. Besides its big size, the core size is relatively small compared to light water reactor cores. The ELFR has the following features (Alemberti et al., 2013):

- Power: 1500 MWth.
- Fuel: MOX.
- Coolant: Pb.
- Inlet and outlet coolant temperature: 400/480 °C.
- Maximum coolant velocity: 2 m/s.
- Core height: 1.4 m.
- Core diameter: 4.5 m.
- Maximum cladding temperature: 550 °C.
- Total Efficiency: 42%.
- Core breeding ratio ~1.

The ELFR is better known as an adiabatic reactor, where all the transuranic elements (TRUs) are produced and consumed inside the reactor with no exchange of TRUs between the reactor and the environment (closed fuel cycle) (Artioli et al., 2010; Stanisz et al. 2016).

The primary aim of this concept is to demonstrate the viability of a safe and sustainable reactor concept throughout the exploitation of the characteristics linked to the intrinsic properties of lead, as well as achieving economic competitiveness (Grasso et al., 2013b). The ELFR concept is being developed under the LEADER project headed by Italy along with a European consortium of universities and research facilities (Grasso et al., 2013b).

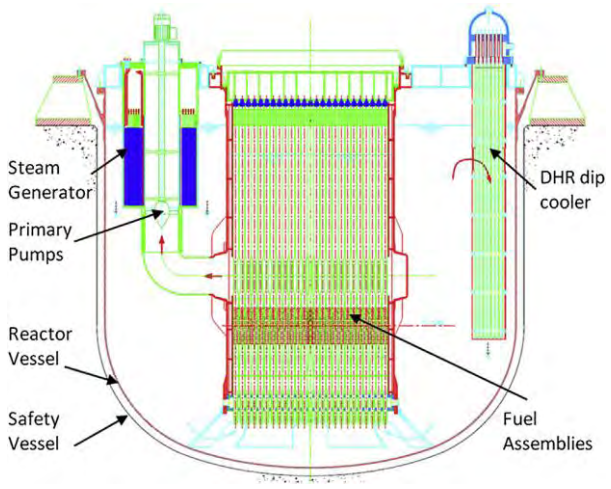

Figure 7. ELFR configuration (Alemberti et al., 2013).

1.1.5. Other prototypes

The **SVBR-100** is a 100 MWe Russian modular reactor cooled by Pb-Bi. It allows the use of a wide variety of U-Pu fuels such as uranium oxides (UO), mixed oxide fuels (MOX), uranium nitride (UN), U-Pu nitride (UN-PuN), and a mixture of ^{232}Th-^{233}U fuels (Toshinskyab et al., 2013).

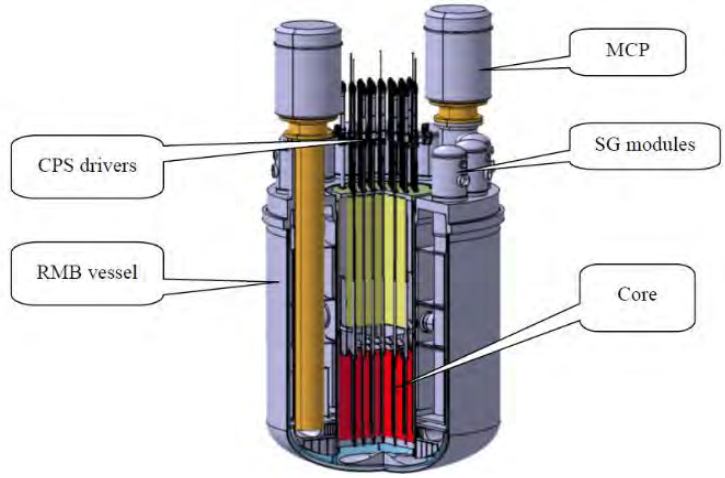

Figure 8. SVBR-100 reactor (Toshinskyab and Petrochenko, 2012).

CLEAR (China LEad Alloy cooled Reactor) is an Accelerator Driven System (ADS) designed by China. This system uses Pb-Bi as the coolant as well as spallation blanket since lead and bismuth can produce abundant spallation neutrons when are hit by energetic protons. Three different models are considered (Wu, 2016):

1. A 10 MWth Pb-Bi reactor coupled with an ADS system where the protons energies range from 50-250 MeV.
2. An experimental reactor of 100 MWth with an accelerator of 600-1000 MeV/10 mA. It is planned for the year 2020.

3. An ADS demonstrator installation with a high capacity for nuclear waste transmutation. The reactor has Pb as the coolant as well as spallation blanket. The protons energy is about 1.5 GeV/10 mA, planned for the year 2030.

Fig. 9 shows the reactor layout.

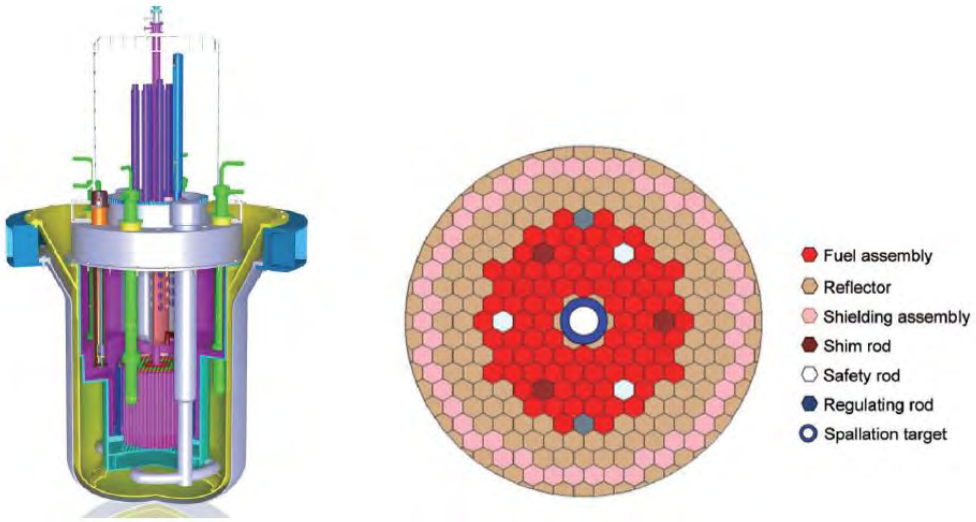

Figure 9. CLEAR reactor and core layout (Wu, 2016).

MYRRHA (Multi-purpose hYbrid Research Reactor for High-tech Applications) is a flexible experimental ADS system able to operate in critical and subcritical mode. The main purpose of MYRRHA is to perform experimental analysis in order to develop new fuel technologies, materials for GEN IV power reactors, materials for fusion reactors and minor actinides transmutation. MYRRHA is based on the Pb-Bi technology, and it will play an important role in the development of the LFRs technology (Abderrahim et al., 2012). **Fig. 10** shows the reactor core layout.

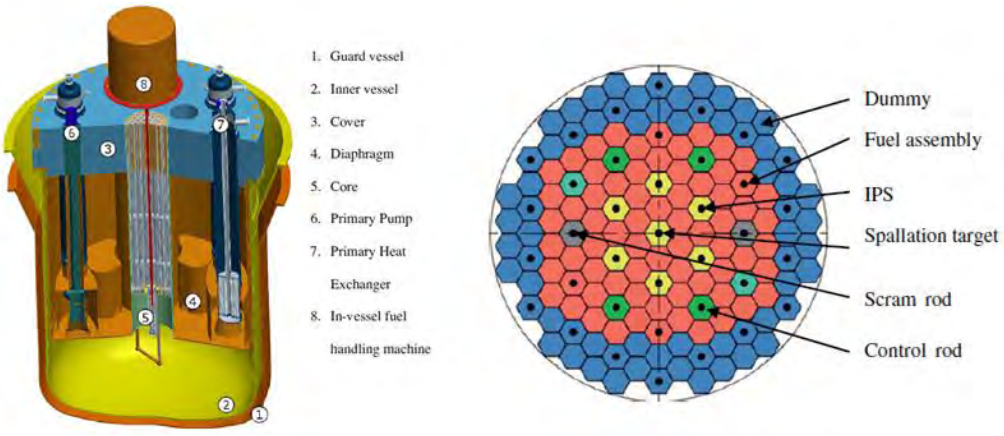

Figure 10. MYRRHA layout (Abderrahim et al., 2012).

All the aforementioned concepts and prototypes are the main LFR systems around the world and a lot of work is being performed under several international programs with the aim of reaching a commercial level in the near future.

The European Union recognized that nuclear energy would play an essential role in maintaining the security of energy supply, limiting greenhouse gas emissions as well as safeguarding economic competitiveness. Then, the R&D of the new generation of nuclear power reactors, to be possibly built and operated in Europe in the long term, has been adopted in a Strategic Research Agenda (SRA) in 2009 (Grasso et al., 2013b).

It is expected that sodium fast reactors will be the reference technology for the Europe fast reactors fleet in the future, mainly because of the much experience gained in this technology since last century. Along with SFRs, two other reactor technologies are considered: GFR and LFR. One of which will be selected as an alternative solution for the reference SFR technology (Grasso et al., 2013b).

Therefore, the ELFR system was selected for this doctoral research because its relevance in the European Energy Framework and all the progress reached regarding safety, fuel performance, as well as new fuel technologies, will be of great importance for all the LFR systems. More details about the European Lead-cooled Fast Reactor will be discussed later.

Chapter II

Chemical and thermo-physical properties of Pb and Pb-Bi coolants

In a dry atmosphere, lead is practically stainless, while in a humid atmosphere a thin layer of PbO is formed. At 450 °C PbO is transformed into Pb_2O_3, between 450-470 °C is transformed into Pb_3O_4. All these compounds are unstable and will be dissociated into PbO and O_2. On the other hand, lead interacts with water producing $Pb(OH)_2$ in a range of 400-500 °C, but this reaction is not exothermic (IAEA, 2012a).

Natural lead has about 93-99 % of purity, but some impurities such as Cu (1-5 %Wt), Sb, As, Su (0.5-3 %Wt), Bi (0.05-0.4 % Wt), Al, and Au, are found. Otherwise, lead has four stable isotopes: ^{204}Pb, ^{206}Pb, ^{207}Pb, and ^{208}Pb, the last three belong to U, Ac, and Th decay chains, respectively (IAEA, 2012a).

Table 1 shows the main physical and thermophysical properties of lead and lead-bismuth for a typical (Pb 44.5 Wt.% and Bi 55.5 Wt.%) mixture.

Table 1. Thermo-physical properties of Na, Pb, Bi, and Pb-Bi (IAEA, 2012a).

Properties	Na	Pb	Bi	Pb-Bi
Atomic number	11	82	83	---------
Atomic mass	22.9	207.2	208.98	---------
Density at 20 °C [Kg/m^3]	966	11340	9780	10474
Melting temperature [°C]	98	327.4	271.4	125
Boiling temperature [°C]	883	1745	1552	1670
Heat of melting [kJ/Kg]	114.8	24.7	54.7	38.8
Heat of vaporization [kJ/Kg]	3871	856.8	852	852
Prandtl number at 450°C	0.0048	0.0174	0.0135	0.0147
Kinematic viscosity at 450°C [m^2/s]	3E-07	1.9E-07	1.3E-07	1.4E-07

As it can be noticed, the Pb-Bi melting temperature is lower than that for pure lead, which gives a wider temperature range before freezing. Also, less energy is required for the coolant preheating process.

Otherwise, the main problem when Pb, as well as Pb-Bi, are used as coolants is the production of the alpha emitter ^{210}Po, which is produced by neutron capture of ^{209}Bi. Bismuth is an impurity of natural lead when bismuth is enriched for the eutectic mixture (Pb 44.5 %Wt- Bi 55.5 %Wt), the ^{210}Po accumulation is more important, that is why, pure lead is preferred as the coolant and is considered as the coolant for the majority of the LFR concepts. The coolant activation chains are presented next (IAEA, 2012a).

2.1. Lead and lead-bismuth activation chains

Natural bismuth is composed by ^{209}Bi (100 Wt.%), then ^{209}Bi is the most critical impurity for the production of short-term radioactivity in the Pb-Bi coolant. The activation chain is as follows (IAEA, 2012a):

$$^{209}Bi + n \longrightarrow {}^{210m}Bi + \gamma \quad (3)$$

$$^{209}Bi + n \longrightarrow {}^{210}Bi + \gamma \quad (4)$$

$$^{210}Bi \xrightarrow[(5.012\ d)]{\beta^-} {}^{210}Po \quad (5)$$

$$^{210}Po \xrightarrow[(138.4\ d)]{\alpha^+} {}^{206}Pb\ (stable) \quad (6)$$

As is shown in reaction (3), the product is ^{210m}Bi, which has a long half-life $3.3x10^6$ years. This nuclide decays into ^{206}Tl throughout alpha decay. Even if the pure lead is used as the coolant and ^{209}Bi is present as a low impurity, ^{210}Po will be produced after a prolonged time of reactor operation due to bismuth generation by the (n, γ) reaction of the ^{208}Pb nuclide. The activation chain is as follows (IAEA, 2012a):

$$^{208}Pb + n \longrightarrow {}^{209}Pb + \gamma \quad (7)$$

$$^{209}Pb + n \longrightarrow {}^{210}Pb + \gamma \quad (8)$$

$$^{210}Pb \xrightarrow[(22.3\ y)]{\beta^-} {}^{210}Bi + \gamma \quad (9)$$

$$^{210}Bi \xrightarrow[(5.012\ d)]{\beta^-} {}^{210}Po \quad (10)$$

The influence of reactions (7, 8 and 9) in polonium accumulation can be negligible, compared to the accumulation from reactions (4 and 5). The reason why it is assumed as insignificant is due to combined effects: the short half-life of ^{209}Pb (3.25 h) and the long half-life of ^{210}Pb (22.3 years). If the half-life of reaction (9) is compared to the reactor operating time, just a little amount of ^{210}Po will come from ^{210}Pb (IAEA, 2012a).

In a previous study, the accumulation of ^{210}Po was calculated after 40 years of irradiation. When the natural composition of Pb was used, there was an accumulation of ~0.03 g of ^{210}Po at the end of the irradiation cycle. When Pb-Bi was used, about 2 kg of polonium were produced, hence the use of pure lead is preferred over Pb-Bi eutectic. The use of pure lead is considered for the majority of LFR systems (Grasso et al., 2014).

On the other hand, the main gamma emitters in Pb coolant during reactor operation are the following nuclides: ^{207m}Pb, ^{204m}Pb, and ^{203}Pb. After shutting the reactor down, the gamma activity of coolant is produced by impurities and corrosion products such as ^{110m}Ag, ^{124}Sb, and ^{60}Co. Nevertheless, due to

the high density of lead. There is self-absorption of these gamma rays so that the coolant loop requires modest radiation protection (IAEA, 2012a).

Finally, the main β^- emitter during plant operation is due to ^{210}Bi from Pb-Bi alloy. The β^- activity in the primary coolant loop reaches among $2x10^9$ - $5\ x10^9$ Bq/cm^3 (IAEA, 2012a).

The characteristic feature of Pb-Bi coolant is the 5.3 MeV alpha particle from ^{210}Po, which causes that specific safety measures are needed when repair and maintenance tasks in the primary coolant circuit are performed (IAEA, 2012a).

Chapter III

European lead-cooled fast reactor (ELFR)

As was mentioned before, the ELFR is an evolutionary design of the ELSY reactor. The ELSY project started in 2006 and ended in 2010, it means that ELSY design is not pursued anymore, but the activities of the European Lead-cooled Fast Reactor system continue within the LEADER (Lead-cooled European Advanced Demonstration Reactor) project (Artioli et al., 2007; Alemberti et al., 2012a; Alemberti et al., 2012b).

In a critical review of the ELSY reactor, some areas were identified for optimization and subsequent implementation in the ELFR design (Grasso et al. 2013b).

- **Adoption of the 2-batch core**: The ELSY was based on 1-batch core, and the 2-batch core was adopted to improve the fuel burn-up and to reduce the initial reactivity constraint. Then, the ELFR has adopted the 2-batch core with no reshuffling, which means that fuel elements that have been burnt during 1800 days are discharged, and fresh fuel is reloaded.
- **Reactivity control system**: The ELSY control system consisted of 18 control rod banks set in the outer zone of the core, but this configuration pushed the power towards the center of the core increasing the central radial form factor. To deal with that, 12 control rods and 12 safety rods banks were set in the ELFR core configuration, geometrically distributed throughout the core. With more control rods there was a reactivity loss, to overcome this problem, the fuel rods were elongated from 120 cm to 140 cm.

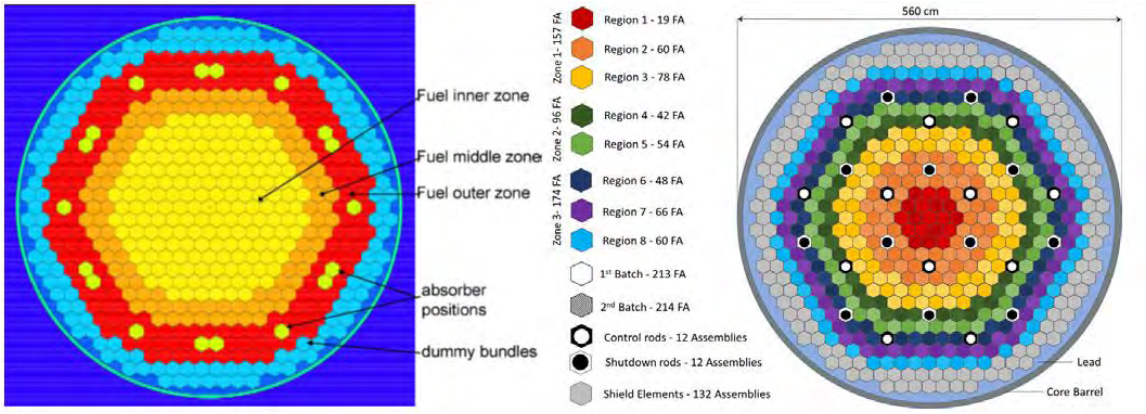

Figure 11. ELSY reactor core (left) and ELFR reactor core (right) (Alemberti et al., 2011; Stanisz et al., 2016).

The ELFR core has been designed under two concepts: the so-called "walk away" and the "adiabatic" concept. The walk away concept refers to have a reactor configuration with passive and intrinsic characteristics to prevent core damage in accident situations with long grace times without the need for any human intervention (Grasso et al., 2013b).

The adiabatic reactor concept refers to have a reactor with an equilibrium fuel in a closed fuel cycle, to minimize the long-live elements present in spent fuel. In this way to fulfill with sustainability goal and waste management requirements for better exploitation of natural resources (Grasso et al., 2013b).

In other words, the adiabatic condition is the state where all the transuranic elements are produced and consumed inside the reactor, with no exchange of TRUs between the reactor and the environment, considering the reprocessing loses (Artioli et al., 2010).

To say that a reactor operates adiabatically some constraints must be met (Stanisz et al., 2016):

- Fuel composition constant from cycle to cycle.
- Constant cycle-to-cycle core criticality at the reference time.
- A core breeding over the whole cycle equal to zero.

Fig. 12 shows the general scheme of an adiabatic reactor.

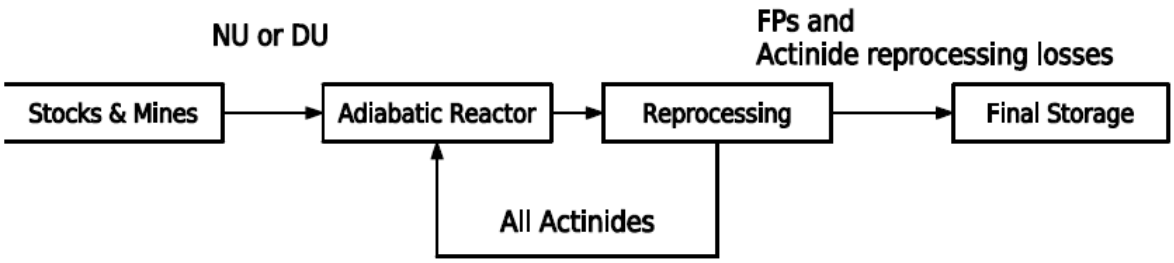

Figure 12. Materials stream in a closed fuel cycle implementing an adiabatic reactor (Grasso et al., 2013b).

3.1. New Paradigm for Nuclear Power

The adiabatic equilibrium state being pursued by the ELFR system imposed a new procedure in designing the reactor core, known as "New paradigm for nuclear power", which applies the following methodology (Artioli et al., 2010):

- First, the unitary cell is designed taking into account the thermal-hydraulic constraint. Geometry gives the neutron spectrum and its intrinsic reactivity.
- Second, the equilibrium fuel composition is defined a priori and adjusted. Then the number of unit cells are determined for criticality as well as the size and power of reactor core.
- Finally, the reactor´s power level is obtained by adjusting the volumetric fraction of fuel of the unitary cell. In this way, the correspondence between the desired power level and criticality is handled.

This methodology is different from that applied for all power reactors, the "old way" to design a core, where core size and power are considered fixed parameters, then the fissile content in fuel is adjusted to reach criticality (Artioli et al., 2010).

The modeling of the adiabatic equilibrium fuel cycle is described next:

The first equilibrium fuel approximation determined a priori is set in the core and irradiated during 900 days. After this time, the first batch (213 FA) is removed from the reactor core, and new fresh fuel is reloaded. Then the fuel burns again for 900 days and the second batch (214 FA) the one that was kept in the core during the first reloading is now extracted and replaced by fresh fuel. The idea is that each fuel batch burns twice to reach a residence time of 1800 days (Grasso et al., 2013b).

Any time, a fuel batch is removed from the core is cooled for 7.5 year, and after this cooling time fission products are replaced by new fuel that could be natural or depleted uranium (NU or DU). The amount of uranium reloaded will be the same amount of mass as the fission products. Then this new fuel composition will be reloaded as the second equilibrium fuel approximation (Grasso et al., 2013b).

The procedure is shown in **Fig. 13**.

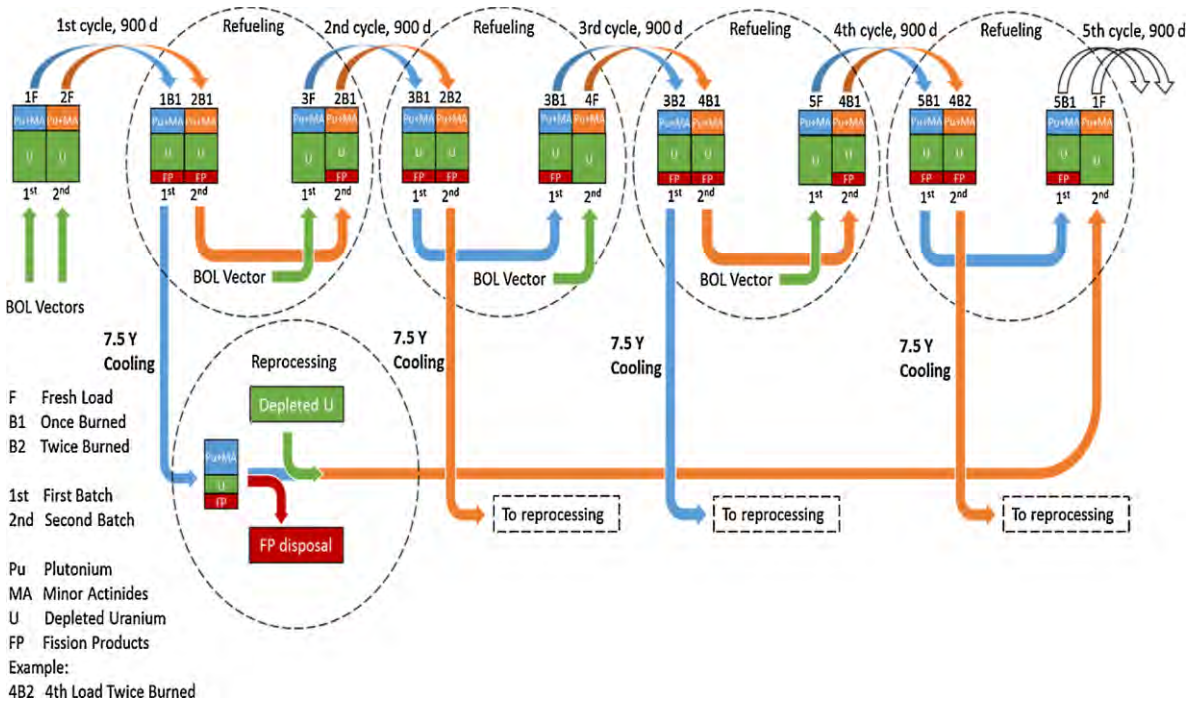

Figure 13. Procedure for modeling of adiabatic fuel composition (Grasso et al., 2013b).

Chapter IV

Thorium fuel

Although the study of thorium began along with the uranium and plutonium applications studies, nowadays there is a renewed interest in the use of thorium as nuclear fuel, especially for GEN IV power reactors (IAEA, 2012b).

This interest is encouraged by the following aspects: thorium is 3-4 times more abundant than uranium over the earth's crust, which would extend the long-term life of nuclear energy. A second incentive is that as nuclear fuel, thorium dioxide (ThO_2) is chemically more stable than (UO_2), besides ThO_2 has a higher melting point (~3370 °C), favorable concerning safety. Finally, a third incentive for the use of thorium is to reduce the spent fuel radio-toxicity. The use of ^{232}Th instead ^{238}U reduces the transuranic elements inventory by two orders of magnitude as well as promotes non-proliferation because less plutonium is produced and ThO_2 is an excellent matrix to incinerate the military and reactor-grade plutonium stockpiles (Juárez-Martínez and François, 2017).

About 6.2 million tons of thorium resources are estimated, and India is the country with the largest thorium reserves, about 846,000 tons, followed by Brazil and Australia with 632,000 tons and 595,000 tons, respectively (WNA, 2017a). **Table 2** shows the worldwide thorium resources.

Table 2. Worldwide thorium resources (WNA, 2017a).

Country	Tons	Country	Tons
India	846,000	Russia	155,000
Brazil	632,000	South Africa	148,000
Australia	595,000	China	100,000
USA	595,000	Norway	87,000
Egypt	380,000	Greenland	86,000
Turkey	374,000	Finland	60,000
Venezuela	300,000	Sweden	50,000
Canada	172,000	Kazakhstan	50,000
Russia	155,000	Other countries	1,725,000

Since India is poor in natural uranium resources and has the largest Th reserves in the world, is making a great effort to commercialize the $^{232}Th/^{233}U$ reactors (Kannan and Krishnani, 2013; WNA, 2017b).

Thorium is a fertile material, which means that it does not undergo fission directly then it needs to be converted into a fissionable nuclide by neutron capture. In this case, ^{232}Th must be converted into ^{233}U which undergoes fission. The process is carried out in the following way: ^{232}Th captures a neutron turning into ^{233}Th, then after 22 minutes ^{233}Th is converted into ^{233}Pa by β^- decay, finally ^{233}Pa is converted into ^{233}U also by β^- decay with a half-life ($T_{1/2}$ = 27 days). A similar process occurs when the fertile nuclide ^{238}U is converted into the fissile isotope ^{239}Pu (NEA, 2015a).

The reaction paths are shown next:

$$^{232}\mathrm{Th} \xrightarrow{(n,\gamma)} {}^{233}\mathrm{Th} \xrightarrow[(22\ \mathrm{min})]{\beta^-} {}^{233}\mathrm{Pa} \xrightarrow[(27\ \mathrm{d})]{\beta^-} {}^{233}\mathrm{U} \qquad (11)$$

$$^{238}\mathrm{U} \xrightarrow{(n,\gamma)} {}^{239}\mathrm{U} \xrightarrow[(23.5\ \mathrm{min})]{\beta^-} {}^{239}\mathrm{Np} \xrightarrow[(2.3\ \mathrm{d})]{\beta^-} {}^{239}\mathrm{Pu} \qquad (12)$$

4.1. Neutronic properties of thorium in fast reactors

It is important to remark that in a fast reactor there are more neutrons than in a thermal reactor, and this is due to the higher number of neutron released by fission and the smaller number of neutrons absorbed uselessly (Jian et al., 2013).

In **Fig. 14**, the following can be observed: at neutron thermal energies, capture cross section of ^{232}Th is about three times higher than ^{238}U, but resonance capture is about three times higher for ^{238}U. In the fast region, the capture cross section of ^{232}Th is slightly higher than ^{238}U, then ^{232}Th is a suitable fuel for fast neutron reactors (Konings et al., 2012; Jian et al., 2013).

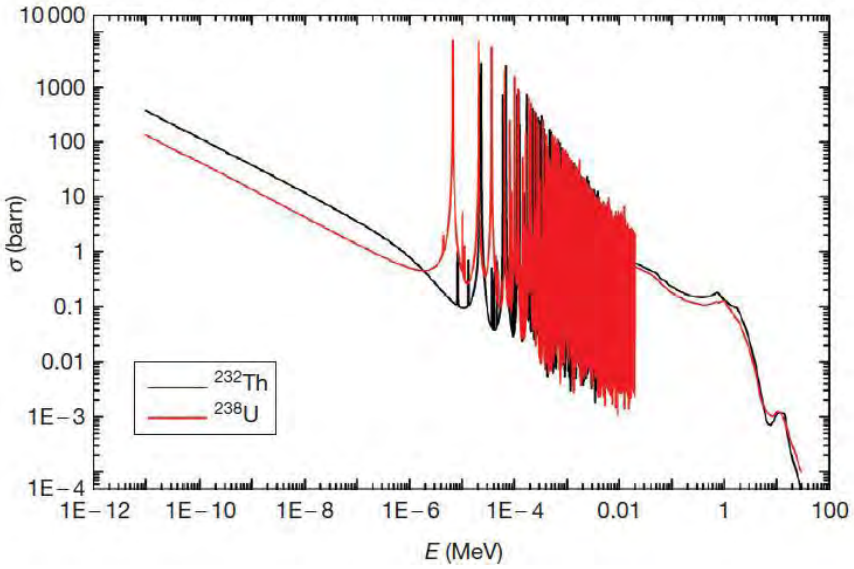

Figure 14. ^{232}Th and ^{238}U capture cross sections in the entire energy spectrum (Konings et al., 2012).

Also, fission cross sections of ^{233}U, ^{235}U, and ^{239}Pu are least dependent on neutrons energy, being relatively small in the thermal region and relatively large in the epithermal and fast regions (Konings et al., 2012), as shown in **Fig. 15**.

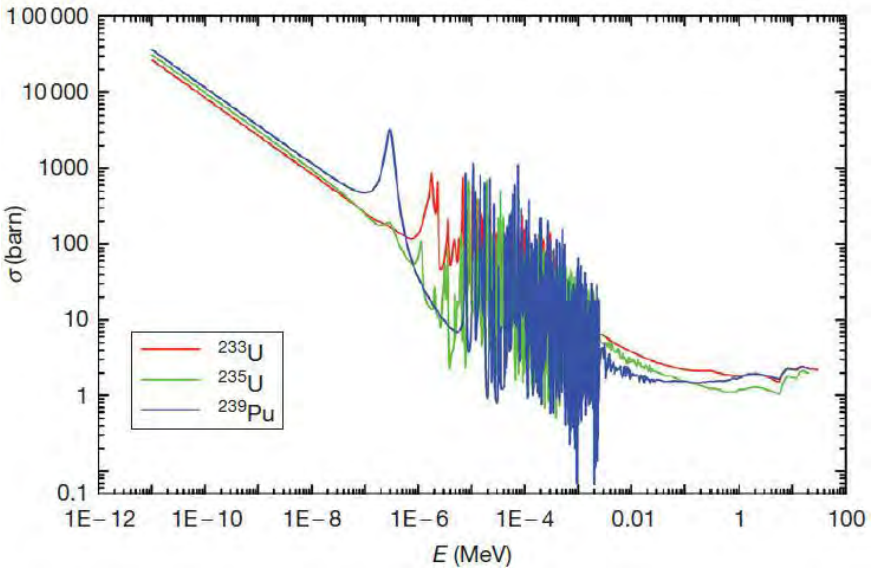

Figure 15. Fission cross section for the main fissile nuclides ^{233}U, ^{235}U, and ^{239}Pu (Konings et al., 2012).

Although several studies have been performed for the implementation of thorium in Boling Water Reactors (BWRs) (Núñez-Carrera et al., 2008), Pressurized Water Reactors (PWRs) (Björk et al., 2013), and Heavy Water Reactors (HWR) (Wojtaszek et al., 2018), the best scenario would be to breed ^{233}U in fast reactors to be burned in thermal reactors, taking advantage of the main features of both reactor systems (Jian et al., 2013).

Nowadays a lot of research is being done to investigate the potential use of thorium in the new generation of nuclear power reactors, mainly focused on MSRs (Heuer et al., 2014), SFRs (György et al., 2017), and GFRs (Shamanin et al., 2018).

As described above, thorium is an excellent candidate as nuclear fuel, and some studies show that the use of thorium instead ^{238}U would extend the nuclear fuel supply from 100 years up to 15,000 years (Serfontein and Mulder, 2014).

Besides, the establishment of thorium fuel cycle depends directly on uranium availability, as well as the extraction costs of the latter. Another barrier is related to spent fuel reprocessing costs to recover the ^{233}U through chemical separation. The approximate cost is ~$1000/Kg (in 2003), then cheaper reprocessing methods are needed (Serfontein and Mulder, 2014).

4.2. THOREX process

The THOREX process is a chemical process alike PUREX process, to separate the fissile uranium from the fertile material, thorium (NEA, 2015b).

The process consists of liquid-liquid separation in two main stages; at first, fission products (FP) are separated from spent fuel composition (Th, U, FP). Then, the uranium is separated from thorium as is shown in **Fig. 16** (Konings et al., 2012).

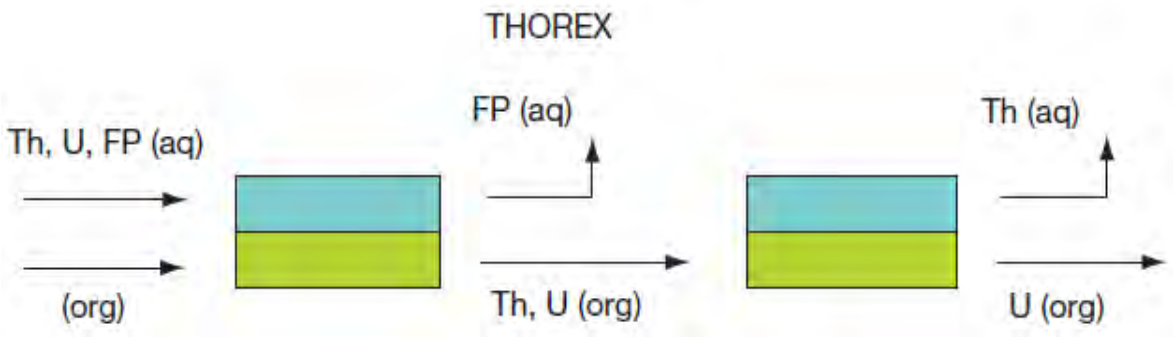

Figure 16. General scheme of THOREX process (Konings et al., 2012).

An essential issue in this process is the presence of uranium fissile in the spent fuel, so this might represent problems related to criticality, reason why reaction devices should be designed to guarantee a safety process (Konings et al., 2012).

4.3. Thorium spent fuel radiotoxicity

Due to ^{233}Pa is the ^{233}U precursor and has a half-life of 27 days, it means that about 12 months of cooling are needed (more than 10 half-lives) before reprocessing, to avoid reactivity problems during fabrication and reprocessing (IAEA, 2005).

Another problem is related to the amount of ^{232}U present in the spent fuel because some of its daughters are high-energy gamma emitters, e.g. ^{208}Tl with a gamma ray of 2.6 MeV of energy; this makes difficult to handle the spent fuel during reprocessing and fabrication, hence a biological shielding and remote handling are necessary (IAEA, 2005).

Finally, after reprocessing thorium contains ^{228}Th with a half-life of 1.9 years, this leaves a radioactive waste for decades, but thanks to its high chemical stability and corrosion resistance, ThO_2 is a suitable waste form (Konings et al., 2012).

In conclusion, the characteristics described above make thorium fuel cycle attractive. The investments in research and development programs related to the continuous use of thorium still go on; as a result, considerable knowledge has been accumulated. Although the experience in manufacturing and irradiation of thorium fuels cannot be considered commercially mature yet, there is enough knowledge and experience today for a viable thorium implementation in a once-through fuel cycle (Konings et al., 2012; Wojtaszek et al., 2018).

Chapter V

Minor actinides transmutation

As is known, nuclear energy production inevitably leads to High Level radioactive Waste (HLW). The management and reduction of HLW is an important issue for the acceptance and future development of nuclear energy (Ivanov et al., 2017).

During the first 100 years, spent fuel radiotoxicity is dominated by fission products (FPs), after this time, actinides, such as (Am, Cm and Np), are the main contributors to the long-term spent fuel radiotoxicity (Kora et al., 2016).

Depending on their half-life, fission products can be classified as Short-Life Fission Products (SLFPs) and Long-Life Fission Products (LLFPs). Regarding SLFPs, ^{90}Sr and ^{137}Cs are the main decay heat emitters during the first tens or hundreds of years after spent fuel discharge (Zhang, 2012).

On the other hand, LLFPs like ^{99}Tc and ^{139}I represent a more prominent problem not only for their long-term radiotoxicity but also for their geochemical mobility, which poses a challenge for long-term disposal (Yang et al., 2004). **Table 3** shows the main LLFPs and their half-lives.

Table 3. Radiological properties of major LLFPs in PWRs (Yang et al., 2004).

Isotope	Type of Decay	Half-Life [years]
^{79}Se	β^-	$6.5x10^4$
^{90}Sr	β^-	29
^{93}Zr	β^-	$1.5x10^5$
^{94}Nb	β^-	$2.0x10^4$
^{99}Tc	β^-	$2.1x10^5$
^{107}Pd	β^-	$6.5x10^6$
^{126}Sn	β^-	$1.0x10^5$
^{129}I	β^-	$1.6x10^7$
^{135}Cs	β^-	$2.3x10^6$
^{137}Cs	β^-	30
^{151}Sm	β^-	89

Although transmutation of FPs is relevant, a typical 1000 MWe PWR generates among 20-30 tons of waste per year, of which about 0.4% of spent fuel mass is long-lived FPs, and plutonium and MAs compose 1% of spent fuel. The relatively lower production and lower radiotoxicity of FPs compared to the MAs make that more efforts are directed towards MAs transmutation (Hu et al., 2017).

In 2006, the MAs storage around the world was about 110 tons plus 40 tons contained as high-level waste from reprocessing. It is estimated that this inventory will double for the year 2020 with the absence of partitioning and transmutation programs, see **Fig. 17** (IAEA, 2009b).

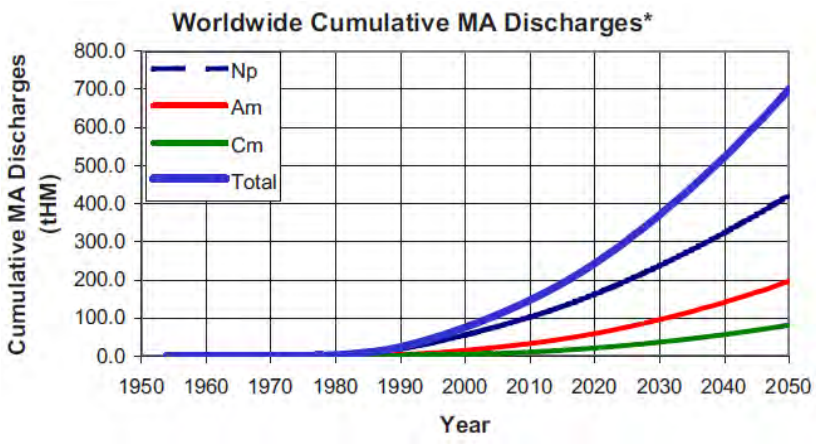

Figure 17. Estimated inventory of MAs worldwide (IAEA, 2009b).

Currently the best option for spent fuel management is the geological repository, but new reactor technologies such as fast reactors are excellent candidates for the management of MAs through transmutation, with the aim of decreasing the amount of nuclear waste while increasing the efficiency of natural resource utilization (Yu et al., 2015; Park et al., 2016).

For MAs transmutation two approaches are being studied, the homogeneous and the heterogeneous fuel configurations. A brief description of each approach is presented below.

5.1. Homogeneous fuel configuration

This fuel is known as MA-Bearing Fuel, where the actinides are set throughout the core, and the amount can range from 1-5 Wt.%. However, this configuration has some limitations that must be considered (NEA, 2014b):

- The core and fuel performance must not be affected by the presence of MAs.
- Fuel pin design must be the same with and without MAs content.
- The burn-up and power reached must be the same as the standard fuel.
- Multiple recycling must be carried out to reduce fuel radiotoxicity.
- The management of minor impurities (lanthanides), resulting from separation process must be guaranteed.

5.2. Heterogeneous fuel configuration

In this configuration, the fuel assemblies loaded with MAs are normally set on the reactor core periphery. This configuration has the advantage of having less impact on reactor operating and safety parameters; therefore it allows a higher MAs content that ranges between 10-20 Wt.%.

However, a drawback of loading the assemblies in the reactor core-periphery is the lower neutron flux compared to the assemblies closest to the center of the core; thus it requires 2 to 3 times more irradiation time than the driver fuel. Also, the flux gradient must be managed to ensure a good transmutation efficiency. Besides, the larger amount of americium results in the larger amount of helium which could be released within the pin's volume free or could cause swelling, and consequently changes in the design of the fuel pin and the assembly, would be needed (NEA, 2014b).

On the other hand, it is a fact that the contribution of Np in LWR spent fuel radiotoxicity is negligible compared to that coming from Am. In addition, the accumulation of Cm is about 1/6 of that of Am, leading to small impact on safety parameters (Zhang et al., 2014). That is why several studies are focused only on the effect of Am in the core safety performance, for example (Zhang et al., 2013; Tesinsky et al., 2012a; Houas et al., 2016).

Considering the aforementioned, in this Doctoral research only Am is considered and its main characteristics are presented next.

5.3. The impact of Am transmutation

When Am is added into the reactor core, some safety parameters are degraded: the Doppler feedback, the void worth, and the effective delayed neutron fraction (Zhang et al., 2014). A brief description of each effect is given next.

5.3.1. Doppler feedback

It is known that in a nuclear reactor when materials temperature changes their cross sections changes too. For example, when fuel temperature increases the resonances of the cross sections in the epithermal energy region become wider, increasing the neutron capture probability. In other words, in a broader energy spectrum, more neutrons can be captured in the core, which leads to a reduction of the effective neutron multiplication factor.

The presence of Am in the fuel will affect the Doppler feedback, mainly by two effects: at first, the higher capture cross sections of Am nuclides, compared to ^{238}U, causes that more neutrons are captured at energies above resonances (~100 keV), causing a reduction in the Doppler constant because fewer neutrons will enter at resonances region. Secondly, Doppler constant will also be reduced because the resonances broadening effect of Am nuclides is weaker than that for ^{238}U, as seen in **Fig. 18** (Zhang et al., 2012; Wallenius, 2012).

Then, Doppler constant is used to correlate the reactivity change with a fuel temperature change as shown in Eq. 13.

$$K_D = \frac{\rho_2 - \rho_1}{\ln(\frac{T_2}{T_1})} \tag{13}$$

where ρ_1 is the reactivity at T_1 and ρ_2 is the reactivity at T_2.

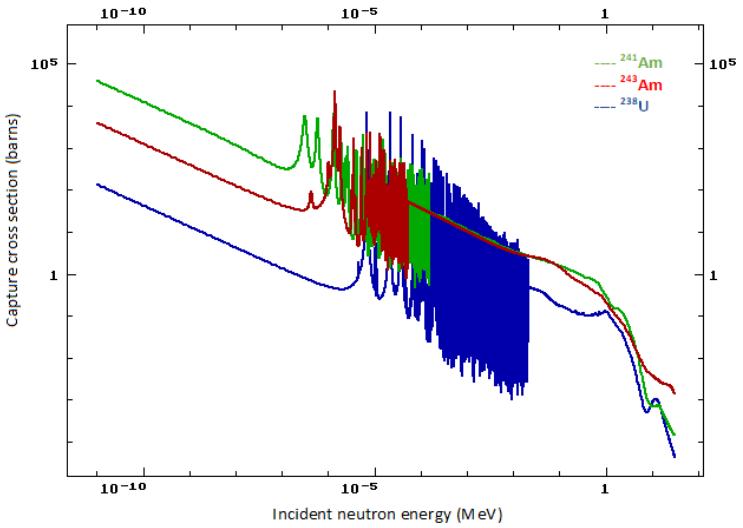

Figure 18. Capture cross sections of ^{241}Am, ^{243}Am, and ^{238}U (ENDF, online plotter, 2018).

5.3.2. Void worth

The variation of coolant density has an impact on reactivity, and this impact is a combination of two effects: the spectral component and the leakage component.

At first, the reduction of coolant density will cause hardening of neutron spectrum due to less neutron moderation, which increases the fission probability of fissile nuclides. This effect introduces positive reactivity to the core. Second, the decrease of coolant density will also cause that more neutrons to escape out of the core due to less interaction among neutrons and coolant atoms, this effect is always negative and more important for small cores (Bortot and Artioli, 2011).

It has been studied that Am nuclides are more sensitive to spectral changes than ^{238}U at $5x10^5$ eV, where ^{238}U is not fissionable yet, increasing the void worth effect, in other words, the void worth effect turns positive with the presence of Am (Wallenius, 2012), see **Fig. 19**.

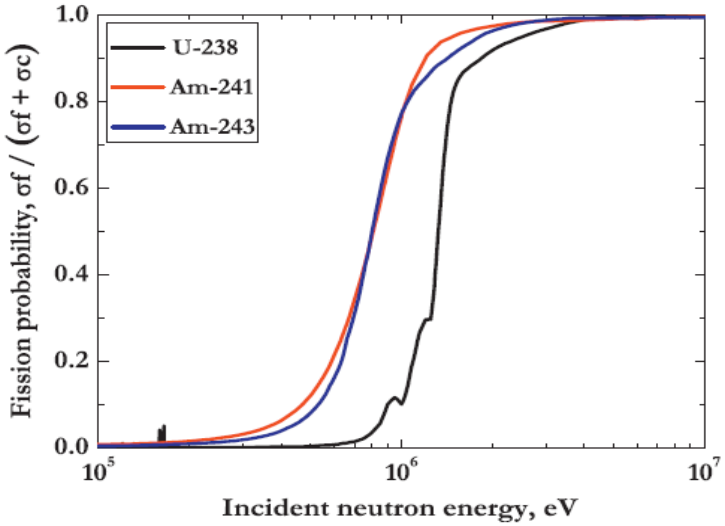

Figure 19. Fission probability of ^{241}Am, ^{243}Am, and ^{238}U (Zhang et al., 2013).

5.3.3. The effective delayed neutron fraction

When fission takes place, prompt neutrons are emitted almost immediately about 10^{-13} s (Tesinsky, 2012b). On the other hand, fission products emit delayed neutrons in longer times after fission, normally in the range of seconds or minutes. Bromine, rubidium, and iodine are the most important delayed neutron precursors (Wallenius, 2012).

The relative fraction of delayed neutrons produced by fission is denoted β. In general, β decreases with the atomic number but increases with the number of neutrons. The highest β value is thus found for ^{232}Th, and the lowest for ^{241}Am and ^{244}Cm, as seen in **Table 4**. Since minor actinides having a mass number higher than that of uranium, the number of delayed neutrons decreases when MAs are added to the fuel (Wallenius, 2012).

Table 4. Delayed neutron fraction for main fissile and fertile isotopes in fast neutron spectrum (Lamarsh and Baratta, 2001; Wallenius, 2012).

Isotope	β (fast neutron spectrum)
^{232}Th	0.0203
^{233}U	0.0026
^{235}U	0.0064
^{238}U	0.0148
^{239}Pu	0.0020
^{241}Am	0.0013
^{244}Cm	0.0013

The fraction of delayed neutrons plays a significant role in the reactor control since this affects the response of the core due to a change in operational conditions. A higher value allows for having longer times for reactivity changes, going from microsecond to seconds or minutes (Grasso et al., 2013b).

The fraction of neutrons that were born delayed and induce new fissions are called the effective delayed neutron fraction (βeff). In a fast reactor $\beta_{eff} < \beta$ (Wallenius, 2012).

The reduction in the βeff is caused by the increment of Am content and fuel burn-up. Since Am nuclides have lower delayed neutron fractions than those of U and Pu, then the presence of Am content will degrade the effective delayed neutron fraction. Additionally, during irradiation ^{238}U will be converted into Trans Uranic elements (TRUs) by neutron absorption and most of the TRUs have lower delayed neutron fractions than ^{238}U, which also degrades the effective delayed neutron fraction (Zhang et al., 2013; Wallenius, 2012).

Chapter VI

Nitride fuels

The study of nitride fuels started in 1960. Nowadays this fuel has been proposed as advanced nuclear fuel, especially for fast reactors. Another interesting application is the use of nitride fuel for space propulsion (Konings et al., 2012).

Compared to other fuels such as oxide, metallic and carbide, nitride fuels have some unusual characteristics. Somehow, we can say that nitride fuels have the advantages of oxide and metallic fuels, due to their high melting point (3053 K) which is close to that for oxide fuels (3083 K), which is good in terms of safety, see **Table 5**. In addition, nitride fuels have a thermal conductivity higher than that of oxide fuels, which allows for operating at higher power densities, up to ~70 W/cm (Konings et al., 2012; NEA, 2014b; Matveev et al., 2015).

Moreover, nitride fuels have a high density (~13.5 g/cm^3) comparable to metallic fuels (14.5 g/cm^3), see **Table 5**. This feature allows for having a lower inventory of fissile material with an enhanced neutron economy that leads to an improved breeding ratio and a more extended cycle operation. Besides nitrides can stand a hard neutron spectrum needed for an efficient transmutation (Konings et al., 2012; NEA, 2014; Matveev et al., 2015). All these are reasons why nitride fuel has a significant potential for MAs transmutation.

Even though metallic fuels can reach high burn-up and have a thermal conductivity higher than oxide fuels, they have a relatively low melting point (~1330 K), additionally, metallic fuels are not compatible with lead or lead-bismuth coolants due to their solubility in this liquid metal in the case of a fuel rod failure. Therefore, for safety reasons, the use of metallic fuels in LFRs is not considered (Loewen et al., 2003).

Table 5. Oxide, metallic, and nitride fuel properties (Konings et al., 2012).

	Oxide fuels	Metallic fuels	Nitride fuels
Theoretical density [g/cm^3]	11.1	15.9	14.3
Metal density [g/cm^3]	9.75	14.3	13.5
Melting temperature [K]	3083	1330	3053
Thermal conductivity [W/m*K]			
at 773 K	4.1	18	15
at 1273 K	2.9	31	18

Finally, carbide and nitride fuels have densities and similar physical properties, since a fabrication point of view, nitrides are easier to fabricate due to carbide fuels have a problem with Am evaporation during the fabrication process and Am is present in plutonium stocks. That is why, nitride fuels seem to be a more realistic candidate as an alternative fuel for lead-cooled fast reactors (Wallenius, 2013; IAEA, 2011).

Nevertheless, one of the main problems with nitride fuels is the formation of ^{14}C by ^{14}N neutron capture, and to overcome this problem, ^{15}N enriched must be used, but this process is expensive yet (IAEA, 2011).

In general, some knowledge has been gained related to nitride fuel thermo-physical properties, but more progress is needed at experimental level especially for a better understanding of their physical properties and its behavior under irradiation conditions. Besides, a cheaper ^{15}N enrichment process is also required (IAEA, 2011).

Taking into account the nitride fuel properties, especially as MAs transmutation matrix, the transmutation of Am in a nitride fuel matrix was performed in this doctoral research. The study is presented in Chapter X.

Chapter VII

ELFR model description

A neutronics modelling of the ELFR in adiabatic equilibrium state has been developed and reported by (Grasso et al., 2013b), study from which dimensions, characteristics, and materials of the reactor were taken.

The reactor core consists of 427 hexagonal fuel assemblies (FA) with an active height of 140 cm. The FA are surrounded by 132 shielding assemblies made of Y-stabilized zirconia. The FA are conformed by 169 fuel pins coated with the Stainless Steel T91, this material was also used as structural material in the modelling process, e.g. channel walls, core barrel, and upper and lower plugs. The core was designed with 12 Control Rods (CR) and 12 Safety Rods (12), which are not modeled in this work.

In addition, two lead densities were set for the neutronics modeling, one of 10.58 g/cm^3 for the inlet region and 10.478 g/cm^3 for the in-core and outlet region, besides a natural lead composition was used taking into account the intrinsic impurities of lead in order to have a more realistic model.

The core was divided into eight radial zones, each of one represented with a different color. The fuel composition is the same for each region, and this radial differentiation is helpful for fuel management.

Finally, the reactor core is submerged in a pool full of lead with a total height of 610 cm, and 680 cm in diameter. The core barrel has 560 cm in diameter with 5 cm in thickness, see **Fig. 20**.

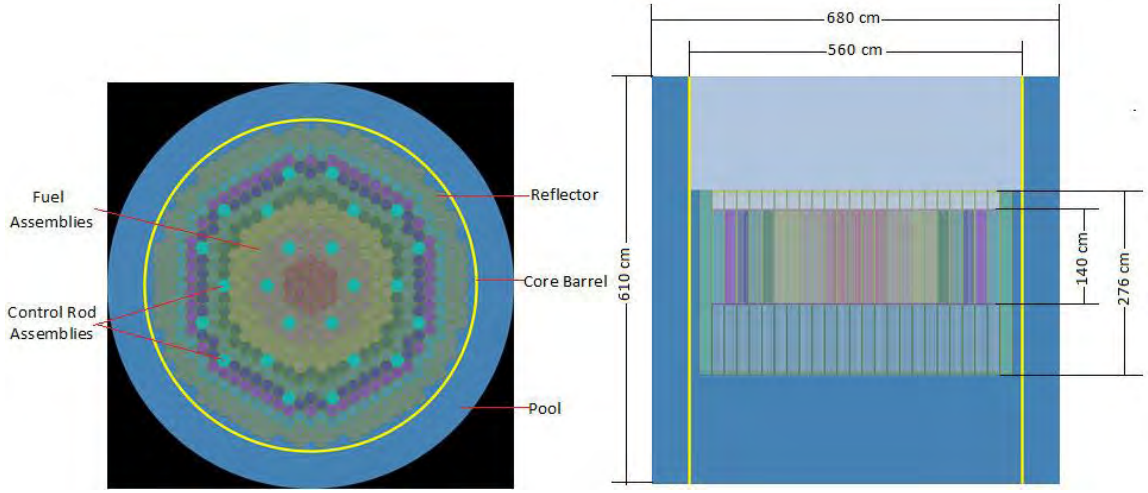

Figure 20. ELFR radial and axial view (Serpent model).

As most of the fast reactors, fuel assemblies have hexagonal geometry as shown in **Fig. 21**.

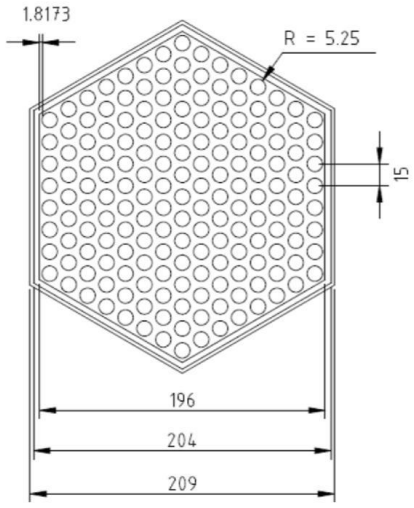

Figure 21. ELFR assembly, dimensions in (mm) (Grasso et al., 2013b).

Fig. 22 shows the fuel rod dimensions.

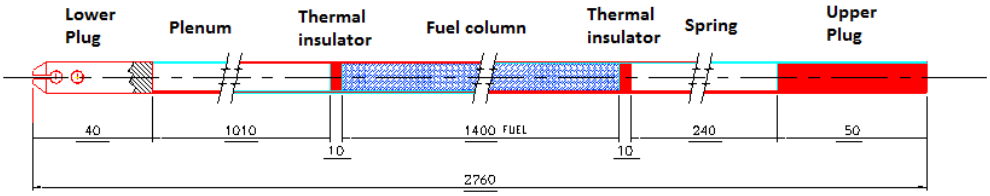

Figure 22. ELFR fuel pin longitudinal view (mm) (Grasso et al., 2013b).

As mentioned in Chapter I, core characterization analyses led to a configuration where the 427 FAs were arranged in two zones: 157 FAs in an "INNER" region, where fuel pellets have 4 mm in diameter hole, and 270 FAs in an "OUTER" region, where fuel pellets have 2 mm in diameter hole, see **Fig. 23**.

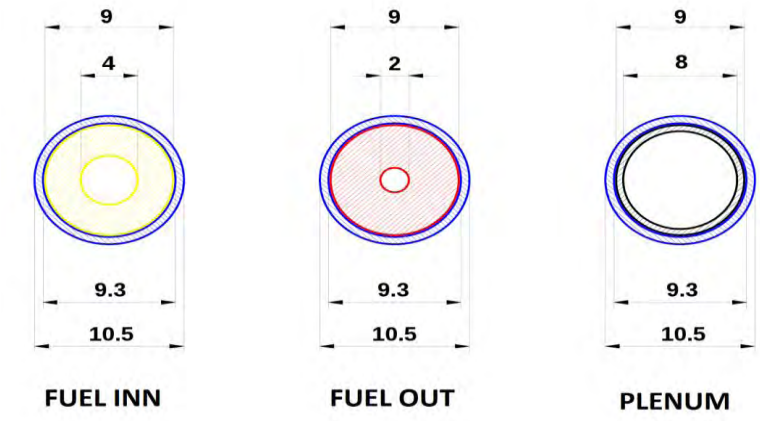

Figure 23. Fuel pin design for ELFR core configuration in the two zones (mm) (Grasso et al., 2013b).

In **Table 6**, the reference equilibrium fuel vector is presented.

Table 6. ELFR fuel vector, equilibrium composition (Grasso et al., 2013b).

Isotope	Wt.%	Isotope	Wt.%
^{230}Th	0.00012	^{242}Pu	0.695
^{231}Pa	0.00001	^{244}Pu	0.00037
^{233}U	0.00002	^{241}Am	0.796
^{234}U	0.247	^{242m}Am	0.026
^{235}U	0.115	^{243}Am	0.209
^{236}U	0.181	^{242}Cm	0.00007
^{238}U	79.910	^{243}Cm	0.0027
^{237}Np	0.109	^{244}Cm	0.0977
^{238}Pu	0.521	^{245}Cm	0.0323
^{239}Pu	9.742	^{246}Cm	0.0223
^{240}Pu	6.773	^{247}Cm	0.0044
^{241}Pu	0.513	^{248}Cm	0.0040

Lead coolant composition is presented in **Table 7**, which includes its intrinsic impurities.

Table 7. Lead coolant composition (ENEA, 2016).

Element	Wt.%	Element	Wt.%
Pb	0.99985	Sn	0.000005
Ag	0.00001	Sb	0.00001
Cu	0.00001	Mg	0.00001
Zn	0.00001	Fe	0.00001
Bi	0.00006	Ca	0.00001
As	0.000005	Na	0.00001

The chemical composition of SS-T91 is presented in **Table 8**.

Table 8. T91 stainless steel chemical composition (Grasso et al., 2013b).

Element	Wt.%
Nb	0.1
Mo	1.0
Si	0.5
V	0.2
Cr	9.0
Mn	0.6
Fe	88.4
Ni	0.2

Finally, the reflector chemical composition is given in **Table 9**.

Table 9. Reflector chemical composition (Grasso et al., 2013b).

Element	Wt.%
O	25.7226
Y	4.0162
Zr	70.2611

A review of all the parameters and materials taken into account for the ELFR modelling are presented in **Table 10**.

Table 10. Main ELFR parameters.

Parameter	
Power [MWth/MWe]	1500/600
Fuel	MOX + MA
Fuel temperature [K]	120
FA geometry	Hexagonal
Coolant	Lead
Number of fuel assemblies	427
Number of fuel pins	169
FA pitch [mm]	209
Pin pitch [mm]	15
Wall channel thickness [mm]	5
Clearance between FAs [mm]	5
Active height [mm]	1400
Hole pellet inner/outer [mm]	4.0/2.0
Pellet outer diameter [mm]	9
Pellet inner diameter [mm]	4
Fuel pin clad thickness [mm]	0.6
Fuel pin gap thickness [mm]	0.15
Number of control rods	12
Number of safety rod	12
Number of shield assemblies	132
Barrel diameter [mm]	5600
Barrel thickness [mm]	50

Chapter VIII

ELFR model validation

The well-known Monte Carlo Serpent code was used in this doctoral research, a brief description of this code is given next.

8.1. Serpent code characteristics

Serpent is a Monte Carlo based code for reactor physics analyses, and it allows for burn-up calculations in two and three dimensions. The Serpent code is the resulting work of the previous Probabilistic Scattering Game (PSG) developed at the VTT Technical Research Centre in Finland. The main difference to the predecessor was the built-in burnup calculation capability, based on two different solution methods of the Bateman depletion equations (Leppänen, 2007).

As other MC codes, Serpent uses a universe based on combinatorial solid geometry (CSG), which allows the description of practically any two or three-dimensional fuel or reactor configuration. The code has the option to define tallies for the computation of the flux, and reaction rates in cells, material, and universes. Serpent reads the continuous energy cross sections from ACE format data libraries. The interaction physics is based on classical collision kinematics, ENDF reaction laws and probability tables sampling in the unresolved resonance region (Leppänen, 2009; Leppänen et al., 2015).

Two methods can be used to solve Bateman´s equations (TTA and CRAM), which describe the changes in isotopic compositions caused by neutron-induced reactions and radioactive decay. The results outputs are written in Matlab m-format files to simplify post-processing data. The code also has a plotter geometry and reaction rate mesh plotter (Leppänen, 2007).

The main advantage of Serpent among other Monte Carlo codes, such as MCNP, relies on speed up calculation which is 5 to 15 times faster than MCNP, and this is due to, at first, the subdivision of cross section energy grid data, which reduces time consumption to find cross sections during transport. Second, the enhanced neutron transport calculation efficiency by combining the conventional ray-tracing and delta-tracking methods (Leppänen, 2009).

8.2. ELFR Modeling and validation

In personal communication with the ELFR core designer Dr. Giacomo Grasso from ENEA, Italy, some changes, in the described above ELFR model, were adopted, to have the most updated ELFR model. These modifications were as follows:

- First, the shielding assemblies length was shortened from 490 to 260 cm of total length, because having shielding assemblies larger than fuel rods have no sense in practice.
- Second, as is shown in previous **Fig. 22**, the thermal insulator length was 1.0 cm, then it was elongated up to 1.5 cm since in practice this is the minimum allowable length to avoid any rotation inside the fuel pin.

- Third, the coolant was divided into three different zones; inlet zone, in-core and outlet zone. Each one has different density value, and these values are reported in **Table 11**.
- Finally, the T91 stainless steel was replaced by the ASS 15-15Ti, because this material was finally chosen for the ELFR model, see **Table 12**.

Table 11. Current ELFR coolant densities (ENEA, 2016).

Zone	Density (g/cm^3)
Inlet	10.5797
In-core	10.52852
Outlet	10.4780

Table 12. ASS 15-15Ti chemical composition (ENEA, 2016).

Element	Wt. %
C	0.00090
Si	0.00850
V	0.00030
Cr	0.14500
Mn	0.01500
Fe	0.65354
Ni	0.15500
Nb	0.00015
Mo	0.01500

The ELFR model validation was performed with Serpent 2.27 version and JEFF3.1 cross sections library. The following neutronic parameters were obtained and compared with the reported values by Grasso et al. (2013b):

- The Doppler constant.
- The reactivity effect of coolant density.
- The effective neutron multiplication factor during 900 days operating cycle.
- The effective delayed neutron fraction and neutron prompt lifetime.

Also, the axial and radial power profiles were obtained and compared with the reference.

8.2.1. Doppler constant (K_D)

To obtain the Doppler constant, three different fuel temperatures were evaluated, 900, 1200 (nominal) and 1800 K. To have a good statistical estimation 1,000,000 neutrons per cycle with 500 active cycles and 50 inactive cycles were simulated. This number of neutron histories was also used to calculate the reactivity effect of coolant density, the effective delayed neutron fraction and the prompt neutron lifetime.

The Doppler constant was obtained at the beginning of cycle (BoC) by using the equation 13.

Considering the aforementioned, it is observed that *keff* values decreased almost linearly with fuel temperature as is shown in **Table 13**. It is observed that *keff* values obtained with Serpent for each fuel temperature are very close to the reference values, with differences that range among 46 to 97 pcm. The Doppler constant obtained with Serpent was -788 pcm which represents a difference of 79 pcm compared to the reported value, see **Table 13**.

The *keff* values obtained with Serpent are slightly above the MCB values, this difference can be due to a difference in the fuel density, since having a higher fission atoms inventory will lead to a higher neutron multiplication factor.

Table 13. keff value and Doppler constant at BoC.

Fuel temp. [K]	[*keff* ± pcm] MCB	Serpent	Difference [pcm]
900	1.00442±10	1.00539±2.5	97
1200	1.00231±10	1.00299±2.5	68
1800	0.99944±10	0.99990±2.5	46

Doppler constant (K_D)		
Reference	Serpent	Diff. [pcm]
-709	-788	79

8.2.2. Reactivity effect of coolant density

In this analysis, the nominal coolant density was set at 10.478 g/cm^3 for all reactor regions, just as was performed by Grasso et al. (2013b). The coolant density was ranged from 5, 25, 50, 75, 95, 100, 105, and 125% of its nominal value and neutron multiplication factor was obtained for each density value.

As mentioned before, the reactivity effect of coolant density on fast reactors has two major effects: The first is the hardening of the neutron spectrum due to less neutron moderation, which increases the fission probability. The second is the increase in neutron leakage due to less interaction among neutrons and coolant atoms (Bortot and Artioli, 2011).

The first effect describes the increment in *keff* among (25-75 %), the second effect describes why *keff* is reduced at the lowest coolant density (5 %) where the amount of coolant is so low that allows the neutrons to travel freely out of the core, since less neutrons are reflected by coolant atoms. Finally, when coolant density is increased the neutrons are somehow moderated (losing energy) due to more neutron to coolant atoms interactions, which leads to a reduction in fission probability.

Table 14 and **Fig. 24** show the Serpent results. The Serpent model has similar behavior than MCB model. As mentioned before, a difference in fuel density can explain why Serpent results are above the MCB results, with differences among 25-787 pcm. The global effect obtained with Serpent was -

105 pcm being less negative than the MCB value. This reduction in the global effect is observed in **Fig. 24**.

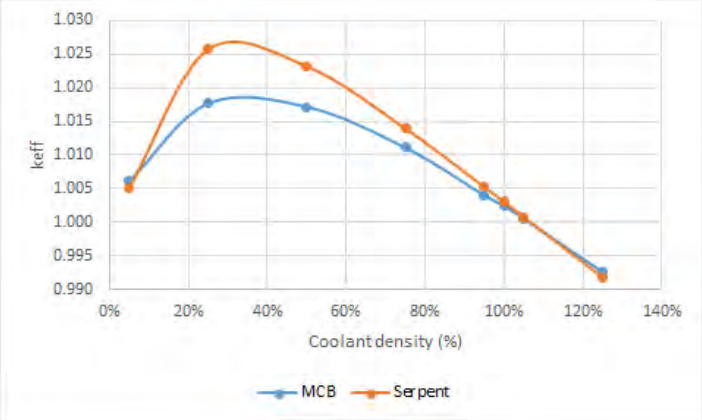

Figure 24. The reactivity effect of coolant density, MCB vs Serpent.

Table 14. Reactivity dependence on coolant density in all regions.

Coolant density [g/cm^3]	[*keff* ± pcm] at BoC MCB	Serpent	Difference [pcm]
0.5239 [5 %]	1.00614±15	1.00517±2.5	96
2.6195 [25 %]	1.01768±15	1.02569±2.5	787
5.2390 [50 %]	1.01716±15	1.02315±2.5	589
7.8585 [75 %]	1.01109±15	1.01392±2.5	280
9.9541 [95 %]	1.00401±15	1.00523±2.5	122
10.4780 [100 %]	1.00243±15	1.00304±2.5	61
11.0019 [105 %]	1.00053±15	1.00078±2.5	25
13.0975 [125 %]	0.99261±15	0.99182±2.5	80
In-core coolant density reactivity effect ([pcm].	-396	-105	291

8.2.3. Criticality evolution

For *keff* evolution, 50,000 neutrons with 150 active cycles and 50 inactive cycles were used, just as was performed by Grasso et al. (2013b). Here the TTA and CRAM methods from Serpent code were used and compared to the MCB TTA burn-up results. The burnup steps simulated with Serpent were the same as the simulated with MCB code; 0, 50, 100, 100, 100, 100, 100, 100, 100, 100, and 50, for a total of 900 days.

Fig. 25 shows the evolution of *keff* during 900 operating full power days. The following can be observed, at first, the results obtained with Serpent (TTA and CRAM) are similar, with differences that range from 3 to 86 pcm. On the other hand, the results obtained with Serpent have the same trend than the MCB values, with average differences of 205 pcm and 216 pcm, for Serpent TTA and CRAM burn-up methods, respectively.

The average burn-up reported by the MCB code was 26.2 MWd/Kg which is higher than that obtained with Serpent code 24.38 MWd/kg, it means that there are less heavy metals in fuel for the MCB model, which confirms a difference in fuel density.

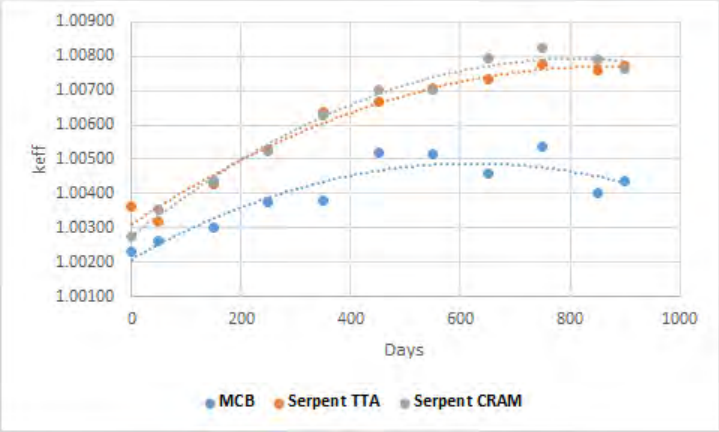

Figure 25. Criticality comparison, Serpent (TTA and CRAM) vs MCB (dotted lines are tendency curves).

The difference among MCB and Serpent burn-up methods is presented in **Table 15**.

Table 15. The effective neutron multiplication factor comparison among MCB and Serpent code.

Days	MCB	Serpent-TTA	Difference [pcm]	Serpent-CRAM	Difference [pcm]
0	1.00231±10	1.00361±21	130	1.00275±21	44
50	1.00264±10	1.00321±21	57	1.00355±21	91
150	1.00301±10	1.00426±21	125	1.00438±21	137
250	1.00376±10	1.00530±21	153	1.00525±21	148
350	1.00378±10	1.00637±21	258	1.00627±21	248
450	1.00521±10	1.00666±21	144	1.00703±21	181
550	1.00513±10	1.00707±21	193	1.00704±21	190
650	1.00457±10	1.00733±21	275	1.00793±21	334
750	1.00535±10	1.00775±21	239	1.00823±21	286
850	1.00401±10	1.00748±21	356	1.00790±21	387
900	1.00438±10	1.00771±21	332	1.00764±21	325

*The MCB results were approximated from a plot reported by (Grasso et al., 2013b), some differences can be expected.

8.2.4. The effective delayed neutron (βeff) fraction and prompt neutron lifetime (Λ)

It is known that reactivity changes occur during normal reactor operation or abnormal or accident conditions, that is why it is essential to see the core response during a reactivity change.

Then, the effective delayed neutron fraction and the prompt neutron lifetime are helpful to know the reactor response when a reactivity change takes place.

The effective delayed neutron fraction and the prompt neutron lifetime, were obtained at BoC and EoC with Serpent code. Unlike MCB or MCNP codes, these neutronics parameters can be obtained directly from the Serpent output, reducing the calculation tasks.

A comparison of βeff and Λ is presented in **Table 16**. It is observed that the results obtained with Serpent are consistent with the reported values, with a smaller 1σ confidence interval than that of MCB.

Table 16. The effective delayed neutron fraction at BoC/EoC.

	βeff [pcm]		Λ [μs]	
	MCB	Serpent	MCB	Serpent
BoC	320±6	321±2.47	0.74±0.2	0.77±0.0004
EoC	332±6	323±2.47	0.83±0.2	0.80±0.0008

8.2.5. Axial and radial power profiles

Fig. 26 shows the relative axial power distribution obtained with MCB and Serpent codes, respectively. It is clear that the axial power profile obtained with Serpent corresponds to a large extent to that reported by Grasso et al. (2013b) with a maximum value of 1.22, the same amount stated.

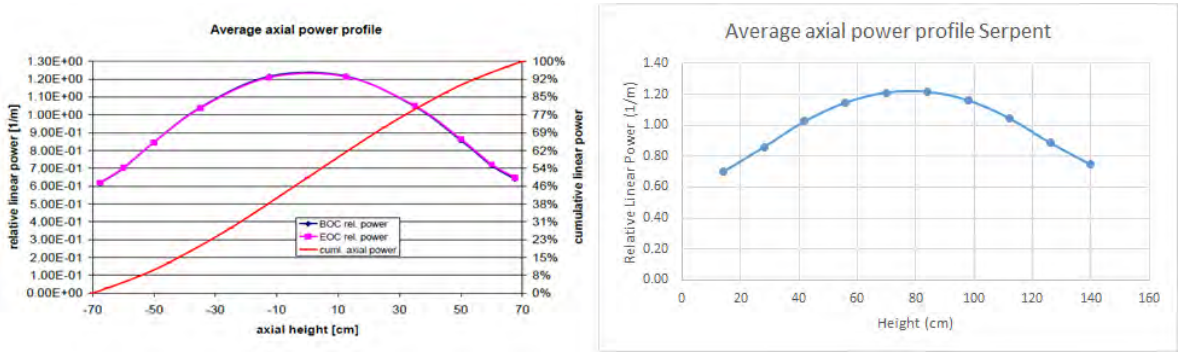

Figure 26. Average axial power profile, MCB (left) and Serpent (right).

Table 17. Average normalized axial power (Serpent).

Axial bin	Average normalized axial power
1	0.70
2	0.86
3	1.03
4	1.15
5	1.21
6	1.22
7	1.16
8	1.05
9	0.89
10	0.75

Finally, for the average radial form factor, the core was divided into eight radial zones (as shown in previous **Fig. 20**). Then the average radial form factor for each radial zone was obtained. Even when fuel composition is the same for each radial zone, this radial distribution is helpful when a fuel management strategy is intended, and it was taken from the reference study (Grasso et al., 2013b).

In **Table 18**, it is noticed that the average radial form factor obtained with Serpent showed a good agreement with the reference values and no significant differences were found. Zone 1 represents the most inner fuel zone and zone 8 represents the outermost fuel zone.

Table 18. Average radial form factor at BoC.

Zone	MCB	Serpent
1	1.35	1.32
2	1.28	1.25
3	1.19	1.18
4	1.27	1.28
5	1.11	1.13
6	0.92	0.94
7	0.67	0.69
8	0.51	0.53

Fig. 27 shows the full core radial power distribution obtained with Serpent code. As it was expected, the highest power generation comes from the center of the core and spreads homogeneously throughout the core.

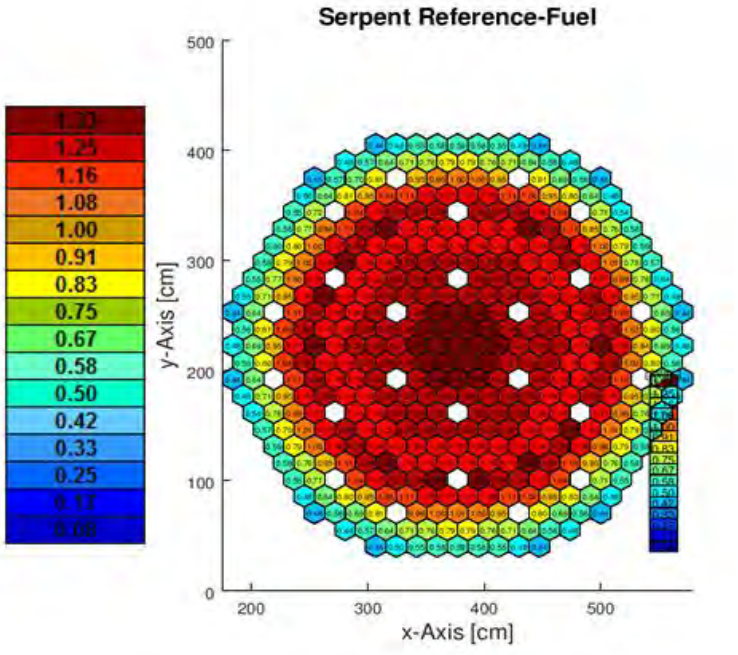

Figure 27. Radial core power distribution obtained with Serpent.

8.3. Conclusions

Once analyzed all the neutronic parameters along with axial and radial power profiles, the following can be concluded: at first, the results obtained with both Serpent methods (TTA and CRAM) are very close one to each other. Then, the trend in the evolution of *keff* obtained with both burn-up modes available in Serpent (TTA and CRAM) was the same than that reported for the MCB code, having average differences for the whole operating cycle of 205 pcm and 216 pcm for TTA and CRAM, respectively. Similar and even slightly greater differences among codes comparison have been reported in other studies (Lopez-Solis, 2016; Ponomarev, 2010).

The difference in *keff* can be due to a small difference in fuel density. Due to the lack of fuel density information in the reference (Grasso et al., 2013b), a standard MOX fuel density was inferred. This fact also explains the difference in average burn-up of about 6.94%, which means that the amount of heavy metals in the MCB model is lower than in our Serpent model, which confirms a difference in fuel density.

Regarding the Doppler constant and the global effect of coolant density, both are near to the expected values with 79 pcm and 290 pcm of difference, respectively. Additionally, for the delayed neutron fraction and the prompt neutron lifetime it was observed that Serpent leads to a good approximation to MCB results and no extra computation was needed since both parameters (βeff and Λ) are easily obtained from the Serpent output file. Finally, the axial and radial power profiles are very close to the reported values.

Therefore, it can be concluded that the model developed with Serpent represents to a large extent the MCB reactor model, taking advantage of its versatility and excellent computing performance. In addition, both Serpent burn-up methods showed to be suitable for the ELFR modelling.

A further job could be the implementation of the two-batch fuel strategy in Serpent code, to analyze the fuel evolution in the adiabatic state condition just as it was performed with the MCB code.

Chapter IX

Thorium fuel analysis

In this part, the main goal was to analyze the core behavior using the fertile material ^{232}Th in the ELFR fuel. For this, two fuel strategies were analyzed, based on the reference fuel vector composed of a mixture of (U/Pu/MAs), which was modified as follows:

- At first, all the uranium isotopes were replaced for a mixture of $^{232}Th/^{233}U$ keeping constant the Pu and MAs vectors, and this fuel composition was called (Th-Homogeneous) fuel.
- At second, three different fuel compositions were set in the core: one with the reference fuel vector (U/Pu/MAs), second with a mixture of ($^{232}Th/^{233}U$/ Pu/MAs), third with ThO_2 as the blanket. Due to the use of different fuel compositions throughout the core, in this case, the fuel was called (Th-Heterogeneous).

In both cases, the *keff* value for 900 days of operating cycle, the Doppler constant and the reactivity effect of coolant density, were obtained. In addition, the axial and radial power profiles, as well as the neutron energy flux, were obtained to complement the neutronic results.

In **Table 19**, the Th-Homogeneous and Th-Heterogeneous fuel vectors are shown.

9.1. Criticality calculations

In this analysis all the uranium isotopes of the reference fuel vector were replaced by a mixture of $^{232}Th/^{233}U$, keeping constant the Pu and MAs vectors. When ^{232}Th was added into the fuel there was a reactivity loss, to overcome with this issue, it was necessary to include the fissile isotope ^{233}U with the aim of providing positive reactivity to the core. Therefore, the $^{232}Th/^{233}U$ ratio was fixed to have a *keff* value greater than one over the whole operating cycle of 900 days.

The *keff* value was obtained with 30,000 neutrons per cycle and 200 active cycles and 30 inactive cycles, with an estimated standard deviation of 21 pcm. This statistic was also used for the Doppler and the reactivity effect of coolant density calculations, for both fuel designs (homogeneous and heterogeneous).

Fig. 28 shows the *keff* evolution for Th-Homogeneous and reference fuel (MOX), both obtained with Serpent code. The following can be observed: during the first 100 days, *keff* value is below the starting point (1.00447±21 pcm), decreasing about 393 pcm; this is because the ^{233}Pa nuclide acts as a neutron poison due to its high capture cross-section, compared to the fertile isotope ^{232}Th, see **Fig. 29**. Although ^{233}Pa has a half-life of 27 days, it takes about 100 days to reach the equilibrium, see **Fig. 30**. After 100 days, the effective neutron multiplication factor starts to increase thanks to the higher production of ^{233}U, then, at about 250 days, *keff* reaches the initial value and then grows progressively until reaching a value of 1.02256±21 (pcm) at the end of the cycle, with a final average burnup of 24.38 MWd/kgU. Similar behavior was reported in another study (György et al., 2017).

It is clear that the evolution of *keff* for the Th-Homogeneous fuel is different from that for reference fuel, with a reactivity difference of ~1400 pcm at the end of the reference operating cycle (900 days).

Table 19. Th-Homogeneous and Th-Heterogeneous fuel vectors.

Th-Homogeneous		*Th-Heterogeneous*					
		Radial Zone [1, 2, 4, 5 and 6]		Radial Zone [3 and 7]		Radial Zone [8]	
Isotope	Wt.%	Isotope	Wt.%	Isotope	Wt.%	Isotope	Wt.%
^{232}Th	78.506	^{230}Th	0.00012	^{232}Th	80.47	^{232}Th	100
^{233}U	1.946	^{231}Pa	0.00001	^{233}U	13.53		
^{237}Np	0.109	^{233}U	0.00002				
^{238}Pu	0.521	^{234}U	0.247				
^{239}Pu	9.742	^{235}U	0.115				
^{240}Pu	6.773	^{236}U	0.181				
^{241}Pu	0.513	^{238}U	79.910				
^{242}Pu	0.695	^{237}Np	0.109				
^{244}Pu	0.00037	^{238}Pu	0.521				
^{241}Am	0.796	^{239}Pu	9.742				
^{242m}Am	0.026	^{240}Pu	6.773				
^{243}Am	0.209	^{241}Pu	0.513				
^{242}Cm	0.00007	^{242}Pu	0.695				
^{243}Cm	0.0027	^{244}Pu	0.00037				
^{244}Cm	0.0977	^{241}Am	0.796				
^{245}Cm	0.0323	^{242m}Am	0.026				
^{246}Cm	0.022	^{243}Am	0.209				
		^{242}Cm	0.00007				
		^{243}Cm	0.0027				
		^{244}Cm	0.0977				
		^{245}Cm	0.0323				
		^{246}Cm	0.0223				
		^{247}Cm	0.0044				
		^{248}Cm	0.0040				

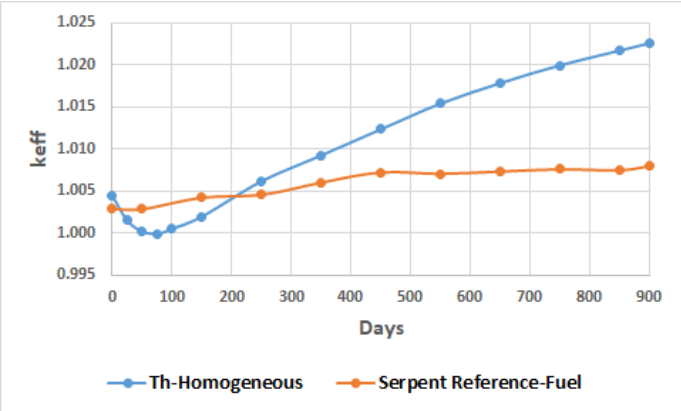

Figure 28. Criticality evolution, Th-Homogeneous fuel cycle (blue), and Serpent reference fuel (orange).

In **Fig. 29**, the values of ^{232}Th and ^{233}Pa capture cross sections are shown. As already described above, the capture cross section values for ^{233}Pa are higher than those for ^{232}Th in the entire energy spectrum of interest (fast region), which explains the reactivity drop during the first 100 days of burn-up.

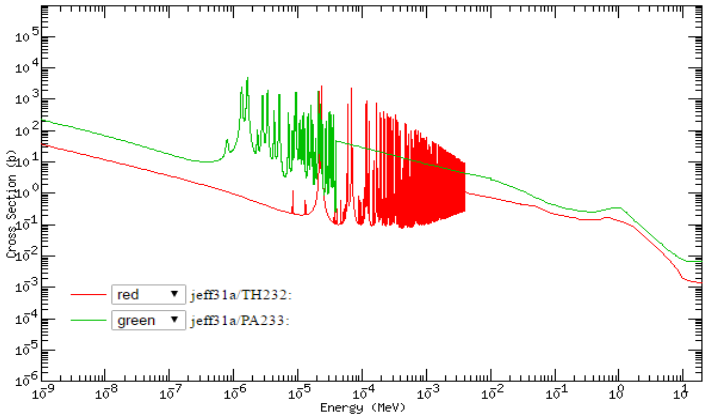

Figure 29. Capture cross section for ^{232}Th and ^{233}Pa (ENDF, online plotter, 2017).

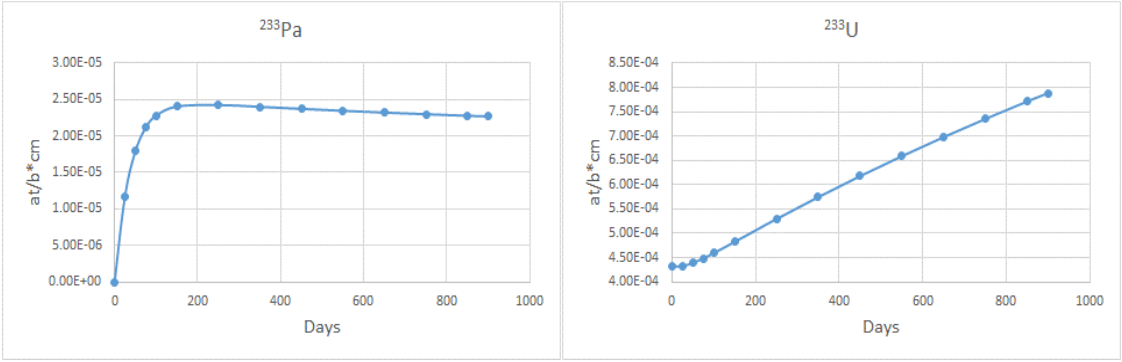

Figure 30. ^{233}Pa and ^{233}U atomic density evolution for Th-Homogeneous fuel.

Regarding Th-Heterogeneous fuel configuration, the $^{232}Th/^{233}U$ ratio from 3rd and 7th radial zones was also fixed to have a supercritical *keff* value during the 900 operating cycle days. The vectors for each radial zone are presented in **Table 20**.

In **Fig. 31**, the effective neutron multiplication factor for the Th-Heterogeneous fuel is presented. The following can be observed: at first, to keep a *keff* value higher than one during the burn-up cycle, it was necessary to have a reactivity excess about 2.22% Δk at BoC. Then, is clear that criticality evolves in a different way than that for Th-Homogeneous fuel; here *keff* value decreases progressively during the burn-up time, starting with a *keff* = 1.02274±21 (pcm), and ending with a *keff* = 1.00198±21 (pcm).

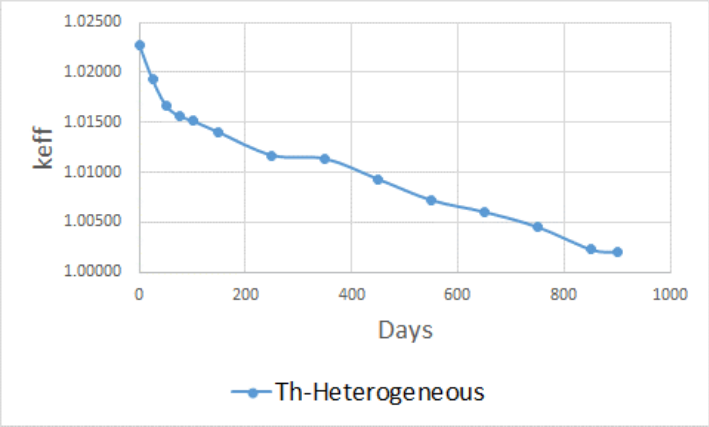

Figure 31. Criticality evolution for Th-Heterogeneous fuel.

This criticality behavior can be attributed to the fact that the amount of ^{233}U present in zones 3 and 7 is being consumed during burn-up, even though ^{233}U is breeding in the 8th radial zone, see **Fig. 32**, the global effect of ^{233}U is not enough to increase the neutron multiplication factor as happened in Th-Homogeneous fuel cycle. **Fig. 33** shows the global inventory of ^{233}U.

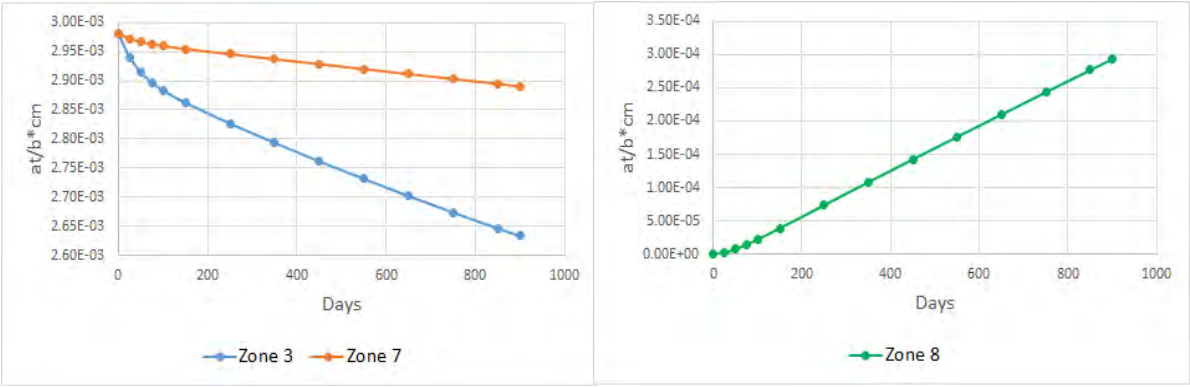

Figure 32. ^{233}U atomic density evolution in 3rd (blue), 7th (orange), and 8th (green) radial zone, for Thorium-Heterogeneous fuel.

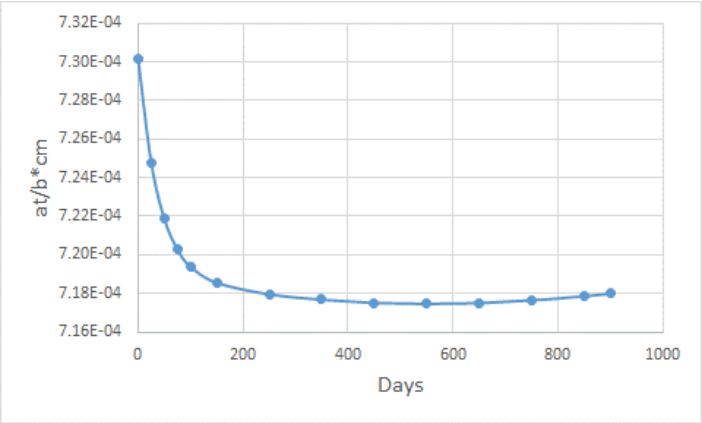

Figure 33. ^{233}U total atomic density evolution for Th-Heterogeneous fuel.

9.2. Doppler constant and reactivity effect of coolant density

In order to calculate the Doppler constant, the neutron multiplication factor was obtained at three different fuel temperatures: 900 K, 1200 K, and 1800 K, where 1200 K is the nominal fuel temperature.

In **Table 20**, the Doppler constant for the entire temperature range and the effect of fuel temperature in the neutron multiplication factor are shown. As it was expected when fuel temperature increases, *keff* value decreases. For Th-Homogeneous fuel configuration, the Doppler constant obtained was -692 pcm, which is 17 pcm lower than the reported reference fuel (-709 pcm). On the other hand, the Doppler constant obtained for Th-Heterogeneous fuel was -562 pcm, this value is less negative than that for the Th-Homogeneous and the reference fuel.

Table 20. The effect of fuel temperature on keff and Doppler constant.

Fuel temperature [K]	Reference [*keff* ± pcm]	Th-Homogeneous [*keff* ± pcm]	Th-Heterogeneous [*keff* ± pcm]
900	1.00442±10	1.00668±21	1.02488±21
1200	1.00231±10	1.00426±21	1.02274±21
1800	0.99944±10	1.00185±21	1.01912±21
Doppler constant:			
[pcm]	-709	-692	-562
[pcm/K]	-0.788	-0.769	-0.624

Regarding the reactivity effect of coolant density, the same values as in the validation were evaluated. The results obtained for Th-Homogeneous and Th-Heterogeneous showed the same trend than the reference fuel, reaching a maximum *keff* value at 50 % of nominal density, afterwards *keff* value decreases almost linearly, see **Table 21**.

Table 21. Reactivity dependence on coolant density.

Density fraction. [%]	Reference [*keff* ± pcm]	Th-Homogeneous [*keff* ± pcm]	Th-Heterogeneous [*keff* ± pcm]
25	1.01768±15	1.01139±21	1.02445±21
50	1.01716±15	1.01586±21	1.03074±21
75	1.01109±15	1.01148±21	1.02757±21
95	1.00401±15	1.00592±21	1.02352±21
100	1.00243±15	1.00423±21	1.02215±21
105	1.00053±15	1.00315±21	1.02101±21
125	0.99261±15	0.99566±21	1.01540±21

9.3. Nuclide inventory

Fig. 34 shows the fuel inventory at EoC for reference, Th-Homogeneous and Th-Heterogeneous fuels. The nuclides ^{232}Th and ^{233}U are only showed for thorium fuel configurations because there is no ^{232}Th in the reference fuel, and the whole Pu vector was compared for the three cases because this vector is in the three fuel configurations.

As it was described above, the ^{233}U production is higher for the Th-Homogeneous fuel configuration, which explains the difference in *keff* behavior compared to the Th-Heterogeneous fuel case. On the other hand, the Pu inventory of both thorium configurations is lower than that of the reference fuel, due to the lack of ^{238}U in the fresh fuel.

9.4. Neutron energy spectrum

The neutron energy spectrum was obtained for inner and outer fuel as well as radial reflector zones (RR). In **Fig. 35**, it can be observed that neutrons energy is higher for the inner fuel, compared to the energy of the neutrons in the outer fuel. Then, the spectrum is a little bit harder in the inner fuel.

This behavior is because in the outer fuel, neutrons loss energy due to their interaction with the reflector, which surrounds the outer fuel zone. In addition, the black curve represents the energy spectrum in the radial reflector for each fuel configuration. The three curves are overlapping (each one in black) and it is clear how neutrons loss energy in this zone, drifting the spectrum to lower energies, and causing the difference in the energy of the neutrons among the inner and the outer fuel.

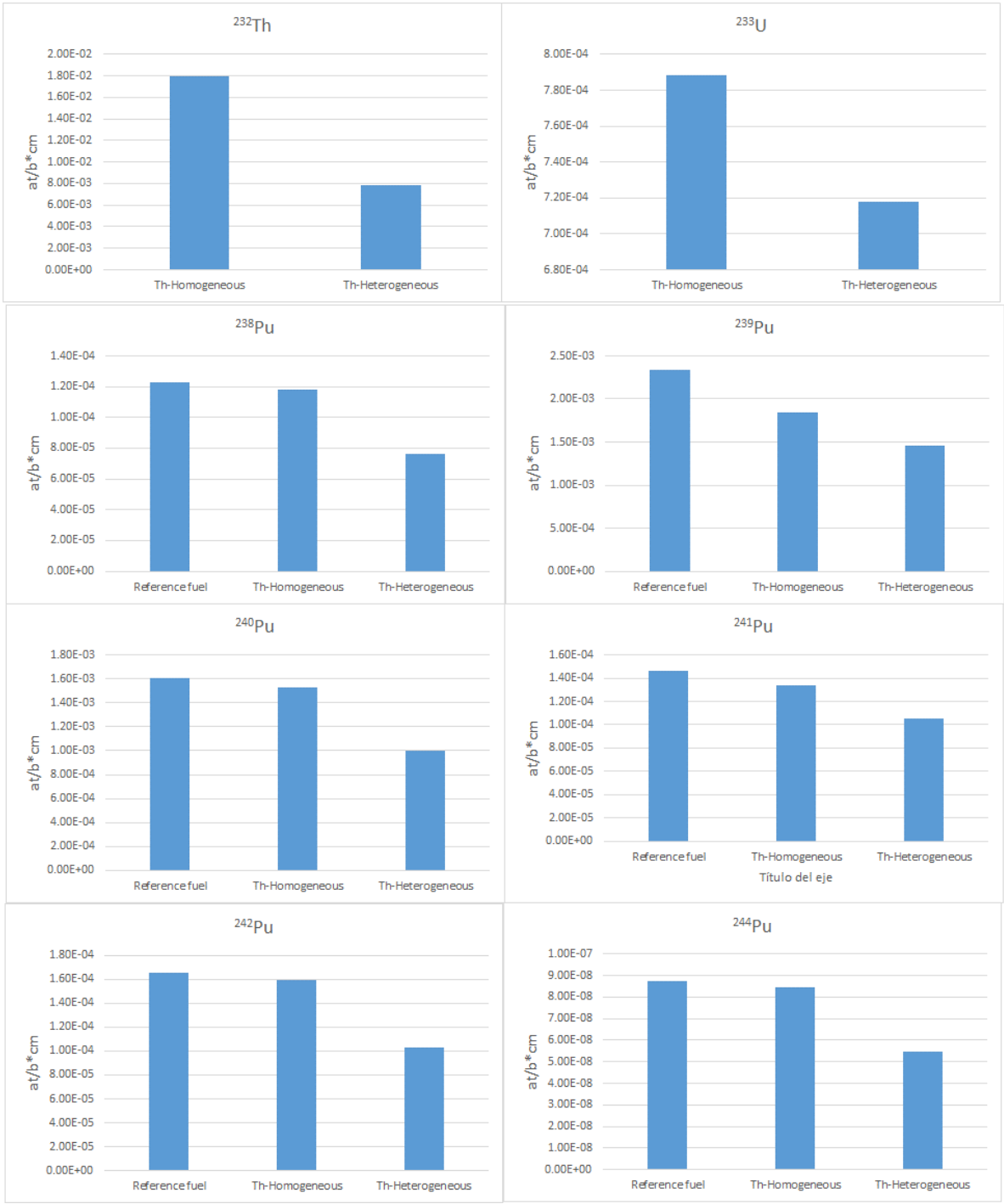

Figure 34. Nuclide inventory at EoC.

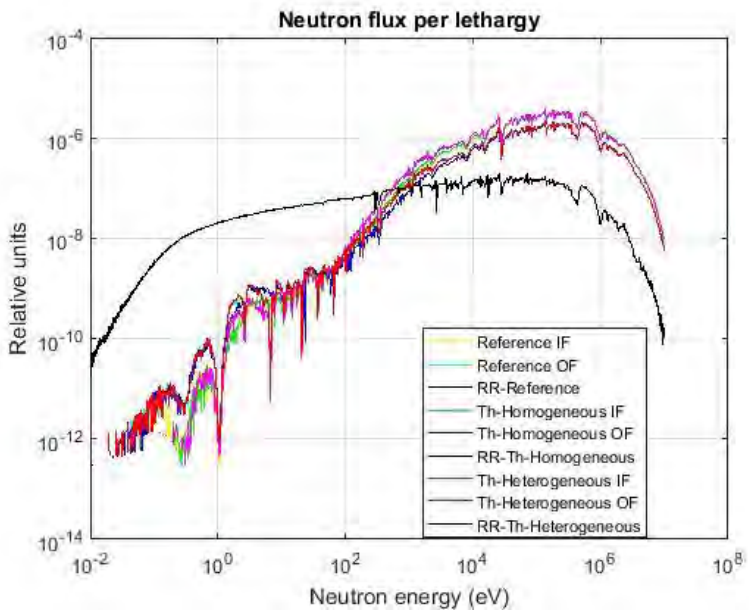

Figure 35. Neutron flux per lethargy.

9.5. Axial and radial power profiles

The average radial form factor was obtained for both cases (Th-Homogeneous and Th-Heterogeneous), respectively. To have a good estimation of the power, 1,000,000 neutrons and 500 active cycles were simulated with an estimated average standard deviation around 0.3%. The average values for the radial form are shown in **Table 22**.

Table 22. Average radial form factor at BoC.

Radial Zone	Thorium Homogeneous	Thorium Heterogeneous	Reference core
1	1.35	1.37	1.35
2	1.28	1.40	1.28
3	1.17	1.75	1.19
4	1.25	1.32	1.27
5	1.10	1.05	1.11
6	0.91	0.74	0.92
7	0.68	0.55	0.67
8	0.52	0.002	0.52

Regarding the Th-Homogeneous fuel configuration, power is distributed homogeneously through the core; then, the addition of ^{232}Th does not affect the radial power distribution significantly due to the values obtained are close to those of the reference core design reported by (Grasso et al., 2013b).

Otherwise, when thorium is heterogeneously added into the core, there are some peaks in the radial power distribution. It can be noticed that the highest power generation comes from the third radial zone filled with a mixture of $^{232}Th/^{233}U/Pu/MAs$ with an average radial form factor of 1.75; this is due to the effect of ^{233}U fissions. In addition, the outer core region (number 8), filled with ThO_2, practically does not generate power due to de lack of fissile material, concentrating the power generation at the center of the core.

It is worthy to underline, that the ELFR core design has a very low average linear heat generation rate (LHGR), 172 W/cm, in such a way that even with a radial power form of 1.75 the LHGR is 317 W/cm, assuming an axial factor form of 1.22 (Grasso et al., 2013b). This value is below the allowed maximum LHGR of 330 W/cm, which has been adopted from the ELSY project. Accident analysis based on this maximum value could demonstrate that fuel melting was avoided in the nominal and the considered DBA transients (Grasso et al., 2013b).

Fig. 36, shows the axial power profile for the three fuel configurations and no differences were found, the three curves are overlapped reaching a maximum relative value at 1.22 as was reported by (Grasso et al., 2013b). Then the use of ^{232}Th did not affect the axial power profile either.

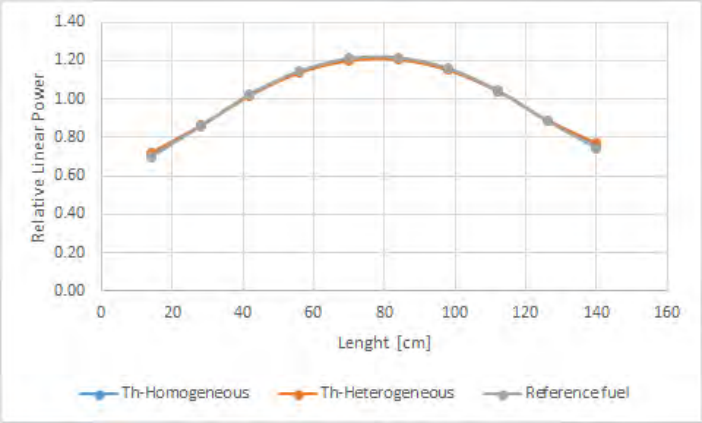

Figure 36. Axial power profile for Th-Homogeneous, Th-Heterogeneous, and Reference fuel.

The full core radial power distributions for Th-Homogeneous and Th-Heterogeneous fuels are presented in **Fig. 37** and **Fig. 38**.

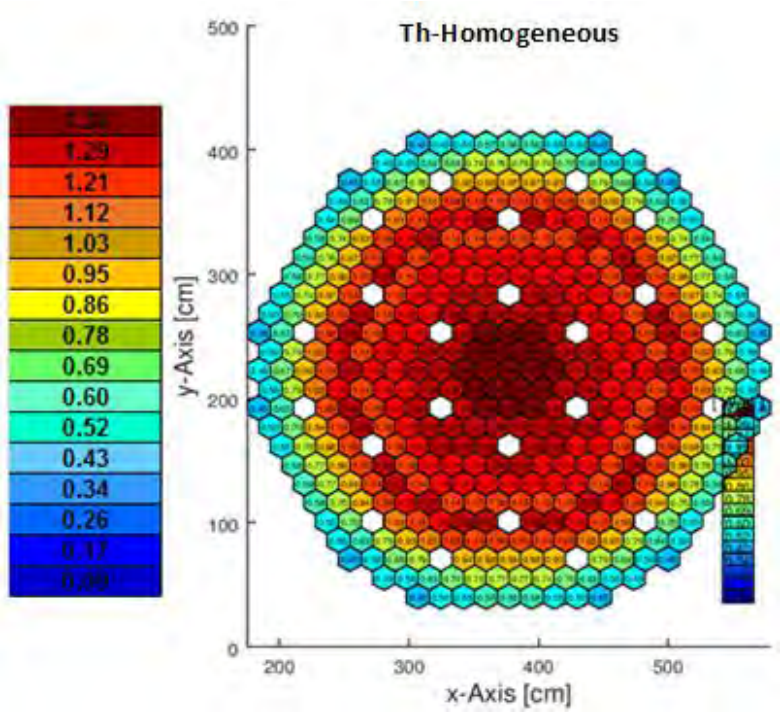

Figure 37. Full core radial power distribution at BoC, Th-Homogeneous fuel.

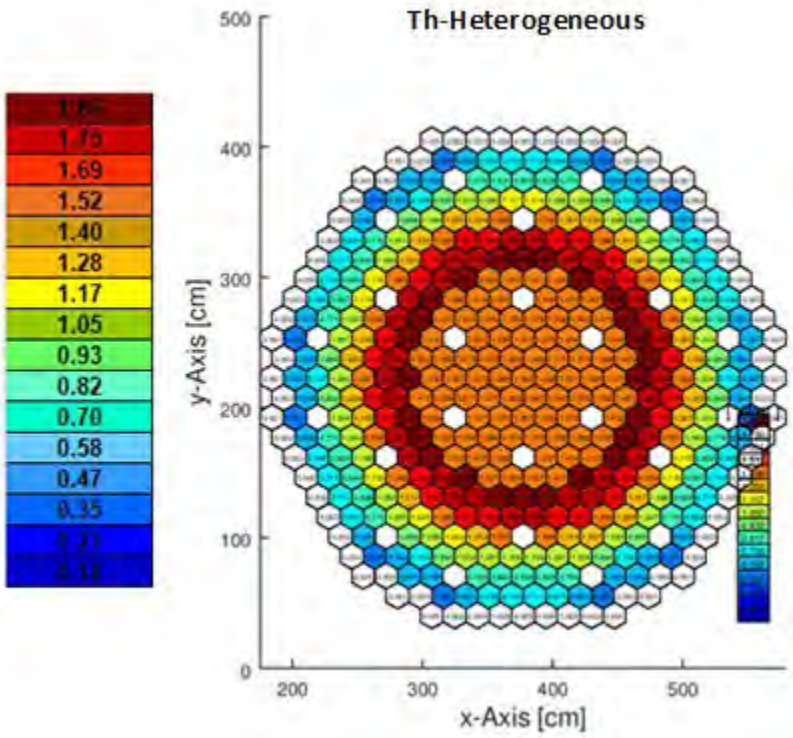

Figure 38. Full core radial power distribution at BoC, Th-Heterogeneous fuel.

9.6. Conclusions

After the analysis of the neutronics parameters aforementioned for the proposed thorium fuel designs, it can be seen that criticality evolution for Th-Homogeneous fuel configuration showed a different trend than that for Th-Heterogeneous fuel, due to the ^{233}U breeding, which provides positive reactivity to the core, which explains the increment in *keff*. This behavior would allow a longer fuel operating cycle than that reported by Grasso et al. (2013b). In addition, as it was expected, the Doppler constant and the reactivity effect of coolant density have negative values being -692 and -148, respectively, and the radial power distribution showed a close behavior compared to the reference model.

Regarding the Th-Heterogeneous design, the reactor starts with a reactivity excess of 2.22% Δk, given by the fissile isotope ^{233}U which was set in the 3rd and 7th radial zones, and this configuration affected the radial power distribution, which had a peak of (1.75) in the 3rd radial zone. Even when there is a breeding zone (number 8), the ^{233}U bred was not enough to increase the criticality causing a drop in the reactivity during the 900 burnup days. On the other hand, the Doppler constant obtained, and the reactivity effect of coolant density remained negative with values of -562 pcm and -84 pcm, respectively.

As a result of this study, it is clear that the best way to breed ^{233}U is spreading the ^{232}Th fertile isotope homogeneously into the core. Further studies, like a transient analysis should be performed to complement this neutronic study. Regarding the heterogeneous fuel core design, an optimization study is envisaged to maximize ^{233}U breeding under linear heat generation constraints for the Th-Heterogeneous fuel design.

Chapter X

Americium transmutation analysis

To analyze the impact of americium in reactor core performance, some safety parameters were evaluated, such as; the Doppler constant, the coolant void worth, and the effective delayed neutron fraction (βeff).

In this study, two nitride fuel configurations loaded with americium were analyzed, which are called; Am-Homogeneous and Am-Heterogeneous fuel.

In both cases, the Am content was ranged as follows: 1, 3, 5, 7, and 9 Wt.%, with the aim of parameterize the impact of Am in core performance. Zhang et al. (2013) analyzed the same amount of Am in a sodium cooled fast reactor, and Tesinsky et al. (2012a) analyzed up to 10 Wt.% of Am content in a lead cooled fast reactor.

A brief description of each fuel configuration is given next:

- For nitride Am-Homogeneous fuel configuration, the Am was loaded homogeneously throughout the core, and Pu vector was fixed at 14.4 Wt.%, to have a supercritical reactor over the whole operating cycle (900 days).
- For nitride Am-Heterogeneous fuel configuration, some americium nitride (AmN) blankets were set in the reactor core periphery. The driver fuel was a mixture of (Du-Pu)N with no Am content. As in the first case, the Pu vector was fixed and set at 13.8 Wt.% to have a supercritical reactor during the 900 days of operating cycle.

In both cases, the Am and Pu vectors were adopted from the spent fuel discharged from LWR after 50 MWd/ kg HM burnup and 10 years of cooling see **Table 23**.

Table 23. Pu and Am vectors from LWRs spent fuel (Zhang et al., 2013).

Isotope	at. %
^{238}Pu	3.50
^{239}Pu	52.88
^{240}Pu	23.82
^{241}Pu	12.90
^{242}Pu	7.90
^{241}Am	57.58
^{243}Am	42.42

The uranium composition corresponds to that for depleted uranium (DU), which contains ^{238}U, ^{235}U, and ^{234}U, with a mass composition of 99.8 %, 0.2%, and 0.001%, respectively (IAEA, 2018).

As mentioned above, the 900 days operating cycle, the time established for the ELFR reference core, was analyzed and all the neutronic parameters were obtained at BoC and EoC.

All the simulations were performed with 30,000 neutrons, 200 active cycles, and 30 inactive cycles, with an estimated standard deviation of 21 pcm. The JEFF3.1 cross section library was also used in this analysis.

10.1. The Am effect in neutron multiplication factor

The effective neutron multiplication factor was obtained at BoC and EoC for both fuel configurations, the results are shown in **Table 24**. The following can be observed: at BoC, the *keff* value decreases when Am content is increased. This is due to Am nuclides have higher capture cross sections than that for ^{238}U and ^{239}Pu nuclides, in the fast region, see **Fig. 39**; which means that having more Am in the fuel, the neutron spectrum turns harder that consequently leads to a reduction of fission probabilities of fissile nuclides, especially ^{239}Pu, the main fission nuclide. Zhang et al. (2013) reported this behavior.

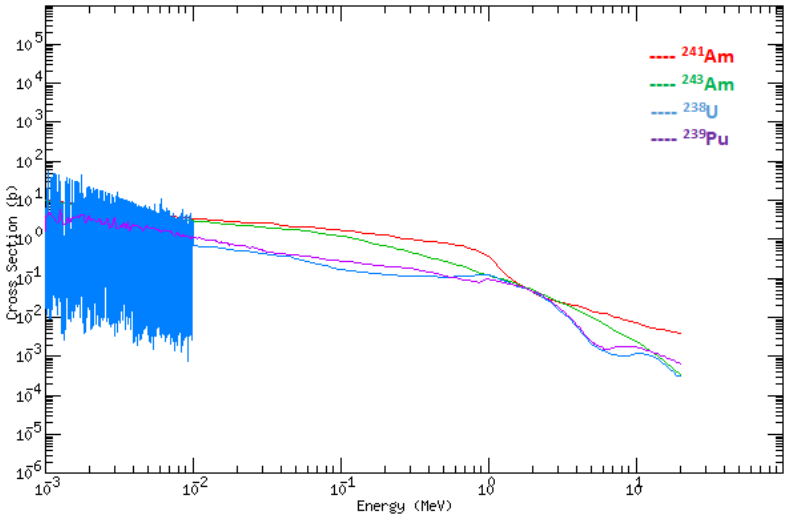

Figure 39. Capture cross section for ^{241}Am, ^{243}Am, ^{238}U, and ^{239}Pu (ENDF, online plotter, 2018).

On the other hand, it can be seen that the neutron multiplication factor increases with Am content at EoC. This effect is caused by some transmutation reactions, such as the formation of ^{238}Pu from ^{242}Cm by alpha decay, where the latest is accumulated due to neutron capture of ^{241}Am, as well as the accumulation of ^{244}Cm from neutron capture of ^{243}Am (Zhang et al., 2013).

Finally, as seen in **Table 24**, the homogeneous distribution of Am throughout the core showed the highest impact on reactivity than that for Am-Heterogeneous fuel configuration. This is caused mainly by the higher Am content and higher neutron flux in the homogeneous fuel configuration. Also, due to neutron flux is lower at reactor edges, the reaction rates will be lower than those at the center of the core.

Table 24. Neutron multiplication factor at BoC and EoC.

	Am-Homogeneous [*keff*±pcm]		Am-Heterogeneous [*keff*±pcm]	
Am %	BoC	EoC	BoC	EoC
1	1.04814±21	1.02814±21	1.01700±21	1.00159±21
3	1.03228±21	1.02136±21	1.01674±21	1.00094±21
5	1.02057±21	1.01648±21	1.01624±21	1.00034±21
7	1.01170±21	1.01176±21	1.01658±21	1.00037±21
9	1.00466±21	1.00873±21	1.01631±21	1.00133±21

10.2. The effective delayed neutron fraction (βeff)

Unlike MCNP code, βeff can be obtained directly from the Serpent output file. In this case, *βeff* was obtained for both fuel configurations at BoC and EoC.

As mentioned in Chapter V, two effects will cause a reduction in *βeff*: the increment of Am content and fuel burn-up. Since Am nuclides have lower delayed neutron fractions than those of U and Pu, then the presence of Am content will reduce the effective delayed neutron fraction. Additionally, during irradiation ^{238}U will be converted into transuranic elements (TRUs) by neutron capture, and most of the TRUs have lower delayed neutron fractions than ^{238}U; both effects explain the reduction in delayed neutron fraction, as seen in **Table 25** (Wallenius 2012; Zhang et al., 2013).

In **Table 25**, this effect is less significant for the Am-Heterogeneous fuel configuration due to the less amount of Am in the fuel. Besides, as was explained in Chapter V, the heterogeneous fuel configuration has a lower impact on reactor performance compared to the Am-Heterogeneous fuel configuration.

Table 25. The effective delayed neutron fraction BoC/EoC.

	Am-Homogeneous βeff [pcm]		*Am-Heterogeneous* βeff [pcm]	
Am %	BoC	EoC	BoC	EoC
1	382	357	385	365
3	377	351	388	365
5	360	337	384	370
7	349	328	385	363
9	338	319	390	362

10.3. Doppler constant (K_D)

In order to obtain the Doppler constant at each Am fraction, four fuel temperatures were evaluated (900 K, 1200 K, 1500 K, and 1800 K) where 1200 K is considered as the nominal fuel temperature for the ELFR reference fuel. To compute K_D the equation 5.1 was used.

In **Table 26**, it is clear how K_D is degraded (turning less negative) with the increment in Am content. As explained before, the higher capture cross section of Am nuclides in the fast region compared to those for ^{238}U and ^{239}Pu, causes that fewer neutrons reach the resonances region, being captured by Am nuclides at energies above (~100 keV), increasing the neutron multiplication factor. In addition, the weaker broadening effect of Am nuclides also contributes to Doppler degradation, as is explained by Zhang et al. (2013) and Wallenius (2012); see **Fig. 40**.

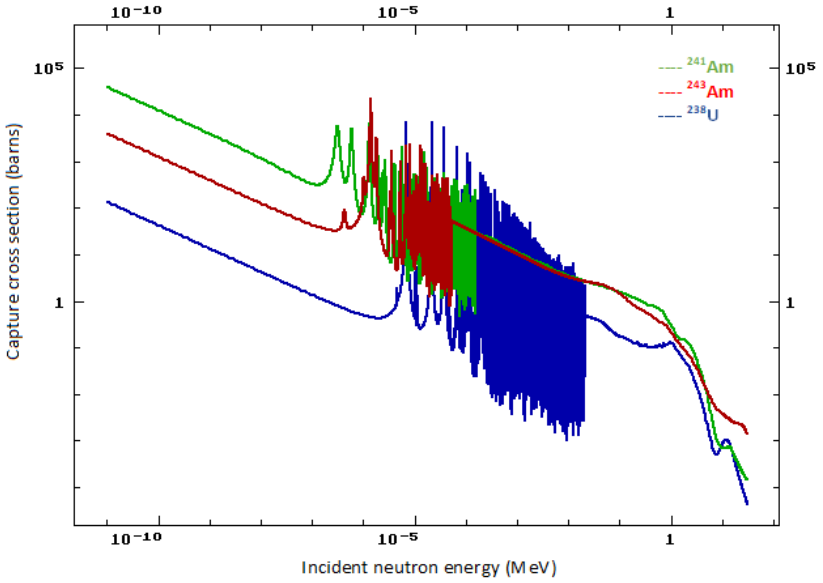

Figure 40. Capture cross sections for ^{241}Am, ^{243}Am, and ^{238}U (ENDF online plotter, 2018).

In **Table 26**, it can be seen how K_D is degraded mainly for the Am-Homogeneous fuel configuration, due to the highest Am content and higher neutron flux.

Table 26. Doppler constant BoC/EoC (pcm).

	Am- Homogeneous		*Am-Heterogeneous*	
Am %	BoC	EoC	BoC	EoC
1	-624	-233	-702	-259
3	-527	-284	-728	-167
5	-302	-149	-709	-210
7	-422	-174	-725	-144
9	-322	-104	-772	-255

10.4. Coolant void worth (W_{Pb})

The coolant void worth was calculated obtaining the reactivity of the unvoided core and comparing it with that of the voided core. As it was explained in Chapter V, the coolant void worth has two major effects: the spectral and the leakage component.

Due to fission probabilities of Am nuclides grows faster than that of ^{238}U after 500 keV (see **Fig. 41**), then Am nuclides are more sensitive to spectral changes. In **Table 27**, it is observed that W_{Pb} turns positive with the increment of Am content, this is due to more fissions from Am nuclides take place when neutron spectrum turns harder and leakage effect becomes weaker, Zhang et al., (2013) and Wallenius, (2012) explained this effect.

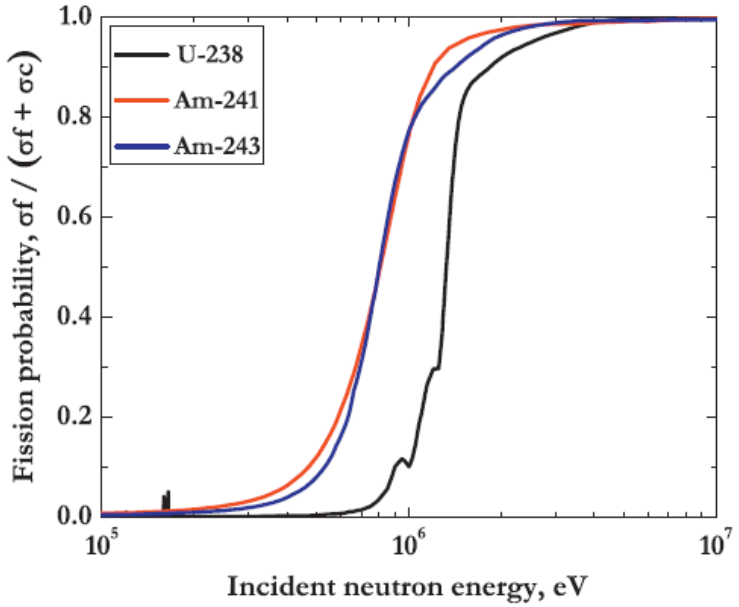

Figure 41. Fission probability of ^{241}Am, ^{243}Am and ^{238}U (Zhang et al., 2013).

The effect is also stronger for the Am-Homogeneous fuel than that of the Am-Heterogeneous fuel due to the highest Am content and higher neutron flux, reaching a positive value of 660 pcm at 9 Wt.% of Am. Which limits the initial Am content as much as 7 Wt.%, in the homogeneous fuel configuration.

Table 27. Coolant void worth [pcm].

	Am-Homogeneous		*Am-Heterogeneous*	
Am %	BoC	EoC	BoC	EoC
1	-2675	-3305	-4252	-5003
3	-1686	-2708	-4277	-5169
5	-826	-2161	-4256	-5188
7	-46	-1518	-4250	-5039
9	660	-800	-4242	-5081

10.5. Consumption of Am

Once the aforementioned neutronics parameters were analyzed, the difference between the initial and final Am content was calculated for both Am fuel configurations. In **Table 28** it can be seen that the highest Am consumption comes from the Am-Homogeneous fuel configuration, and this is due to the higher Am/Pu ratio, and the higher neutron flux which leads to a higher transmutation rate. In addition, the transmutation rate at the edge of the core is expected to be lower than at the center of the core due to the lower neutron flux. This explains why the use of blankets at the periphery of the core needs two to three more irradiation time.

Table 28. Am consumption [BoC-EoC].

	Am 1 Wt.%	Am 3 Wt.%	Am 5 Wt.%	Am 7 Wt.%	Am 9 Wt.%
Am-Homogeneous (g)	-590.4	2530.8	5451.3	8186.6	10755.2
Am-Heterogeneous (g)	379.0	884.4	1167.9	1393.8	1571.9

Negative value means Am production*

10.6. Axial and radial power profiles

For the axial power profile, the active height was divided into ten axial zones. It is observed that the increase in Am content does not affect the axial power profile in both Am fuel configurations. No significant differences were found and it is clear how the curves are overlapped for each Am content, with a maximum value of 1.20 (in both Am fuel configurations), which is slightly lower than that for the reference fuel MOX (1.22), see **Fig. 42**.

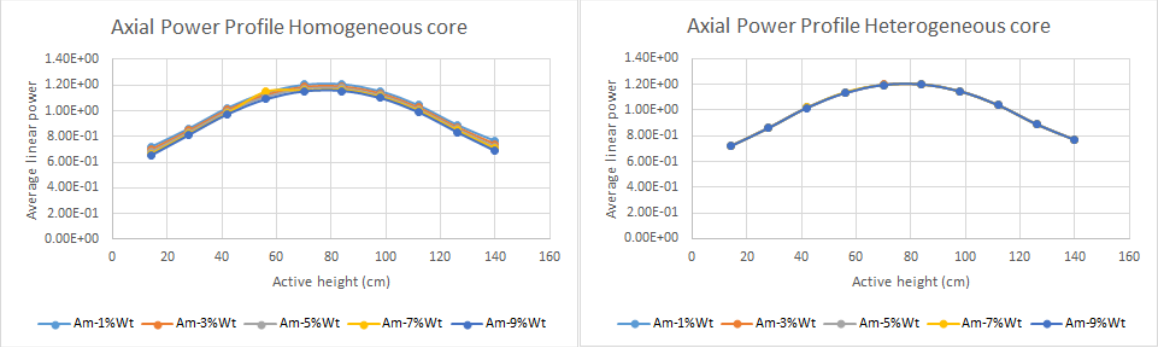

Figure 42. Am-Homogeneous and Am-Heterogeneous axial power profile, right and left, respectively.

For the radial power profile, the core was divided into eight radial zones, just as was performed by Grasso et al., (2013b), for the ELFR reference core. Then the radial form factor was obtained for each radial zone.

For the Am-Homogeneous fuel, power is distributed homogeneously through the core. It is noticed that the average radial form factors of each radial zone are close to those of the reference fuel, with some small differences. Hence, the addition of Am homogeneously does not affect the radial power profile, see **Table 29**.

Otherwise, when Am is set in blanket assemblies, the power generation is pushed towards the center of the core due to the power generation in blankets is too low at BoC, causing an increment in central radial form factors, with a maximum peak of 1.89 (at 5 and 7 Am Wt%), see **Table 29**.

Table 29. Radial form factor for Am-Homogeneous and Am-Heterogeneous.

Zone	Reference fuel [MOX]	*Am-Homogeneous fuel*					*Am-Heterogeneous fuel*				
		1%Am	3%Am	5%Am	7%Am	9%Am	1%Am	3%Am	5%Am	7%Am	9%Am
1	1.32	1.33	1.32	1.31	1.29	1.28	1.85	1.88	1.89	1.89	1.88
2	1.25	1.26	1.25	1.24	1.22	1.22	1.66	1.68	1.69	1.69	1.67
3	1.18	1.17	1.17	1.18	1.16	1.17	1.42	1.42	1.43	1.43	1.41
4	1.28	1.26	1.27	1.28	1.27	1.29	1.37	1.37	1.38	1.38	1.36
5	1.13	1.11	1.12	1.13	1.12	1.14	1.09	1.08	1.09	1.09	1.08
6	0.94	0.93	0.93	0.95	0.94	0.96	0.80	0.78	0.78	0.77	0.77
7	0.69	0.69	0.69	0.70	0.69	0.71	0.42	0.39	0.38	0.38	0.38
8	0.53	0.54	0.53	0.53	0.52	0.53	0.01	0.02	0.04	0.05	0.06

It is worth mentioning, that the ELFR core design has a very low average linear heat generation rate (LHGR), 172 W/cm, in such a way, with the highest radial form factor found (1.89) for the Am-Heterogeneous fuel configuration, the LHGR is 337 W/cm, assuming an axial form factor of 1.20. This value is above the maximum LHGR allowed of 330 W/cm, which has been adopted from the ELSY project.

The core maps for the radial power distribution for each Am content are presented in **Fig. 43** and **Fig. 44**, for the Am-Homogeneous and the Am-Heterogeneous fuel configurations, respectively.

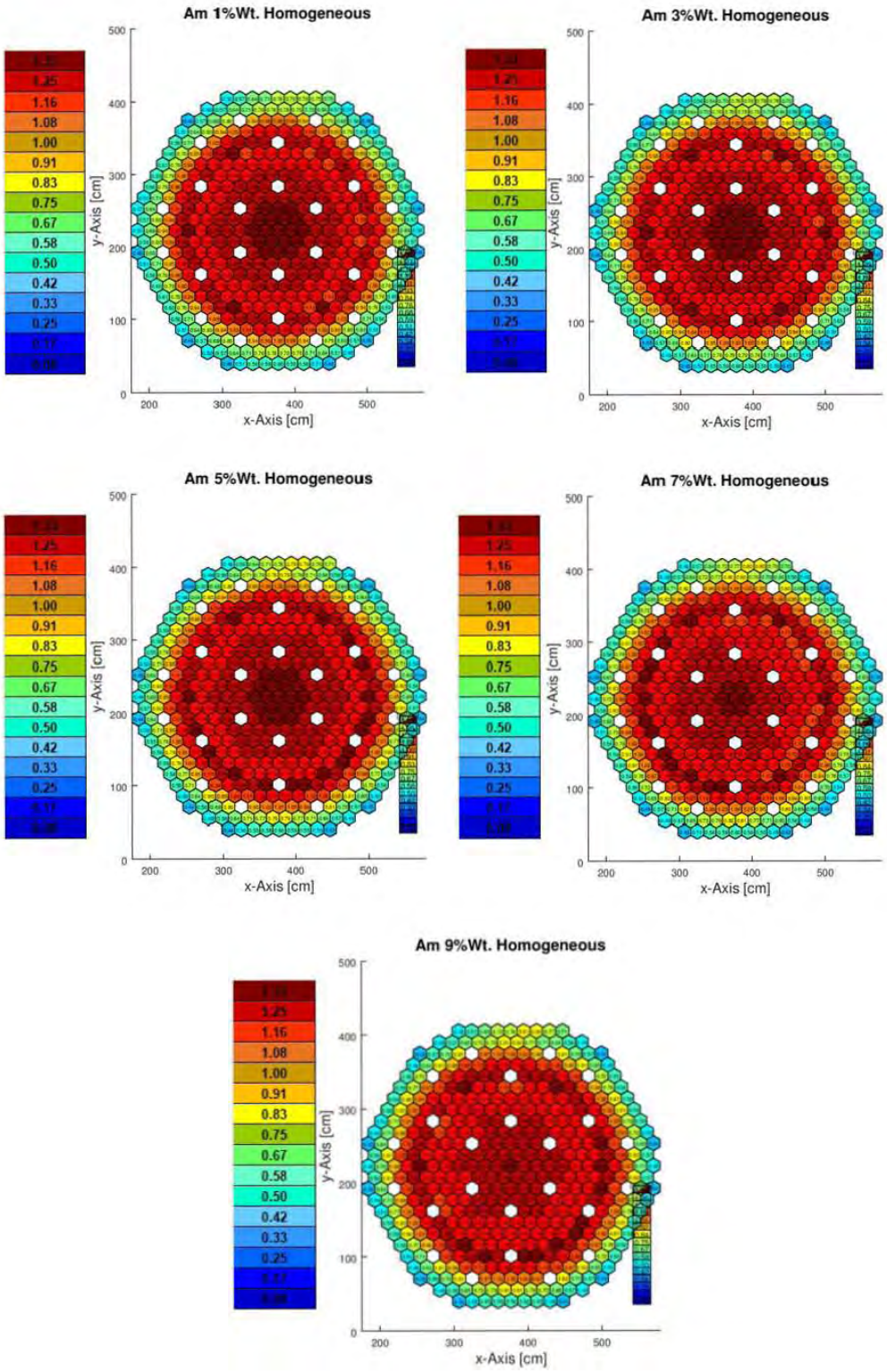

Figure 43. Core maps for radial power distribution, Am-Homogeneous fuel.

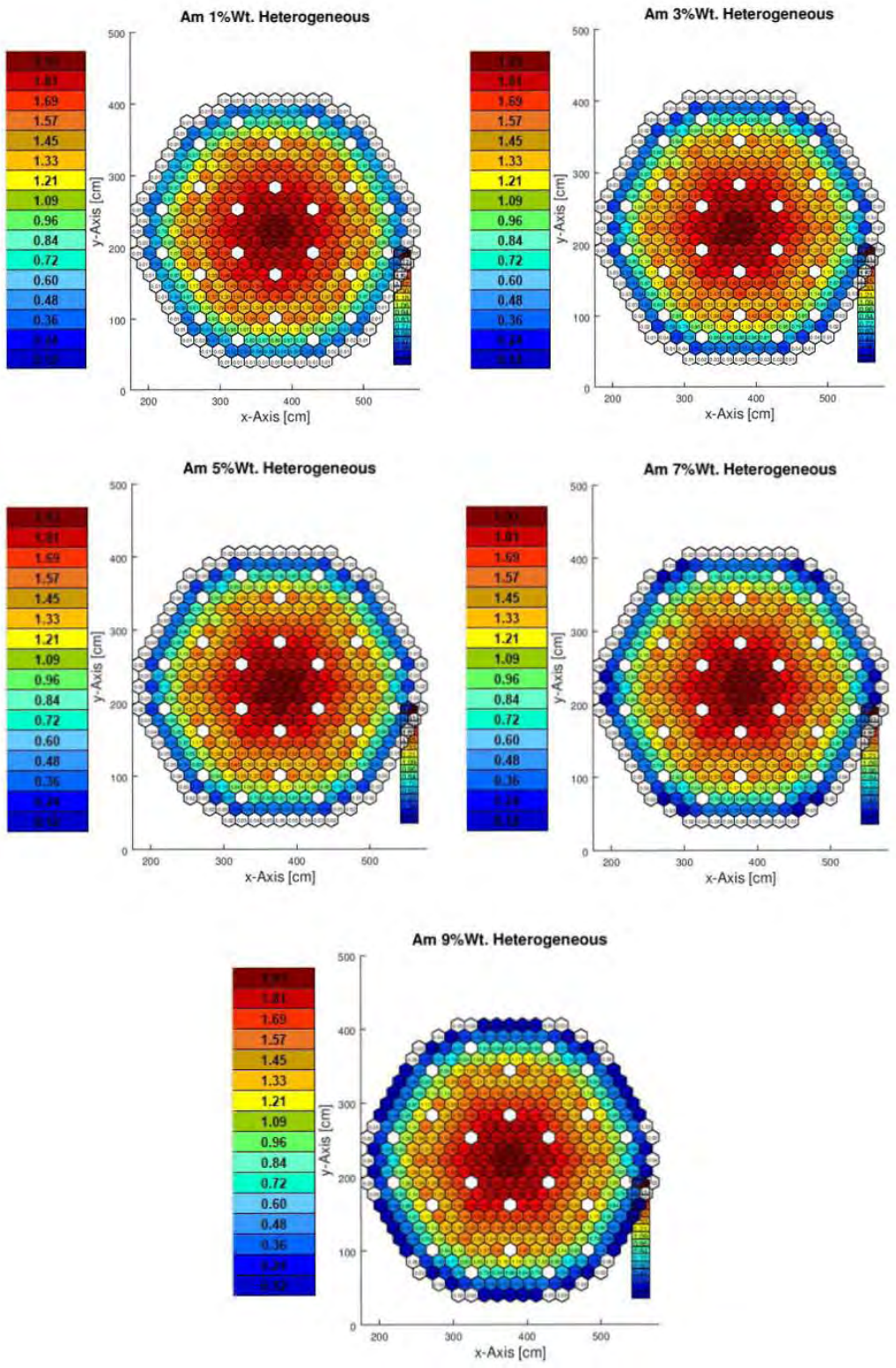

Figure 44. Core maps for radial power distribution, Am-Heterogeneous fuel.

10.7. Conclusions

The impact of Am over the Doppler constant, the coolant void worth, and the effective delayed neutron fraction in the ELFR reactor type, loaded with nitride fuel, was studied for two fuel configurations: Am-Homogeneous and Am-Heterogeneous.

According to the results, for the Am-Homogeneous fuel the Doppler constant was degraded with the increment in Am content having a direct reduction in K_D at BoC and EoC, but in both cases, the obtained values were still negatives, which is good in terms of safety. In addition, the coolant void worth showed a reduction too, obtaining a positive value of 660 pcm at 9 Wt.% of Am content. This affects the reactor safety, which limits the Am content as much as 7 Wt.% at BoC. Regarding the effective delayed neutron fraction, a reduction of 44 pcm at BoC and 38 pcm at EoC was obtained.

The effect of the Am-Heterogeneous fuel configuration had a lower impact over the neutronic parameters than that obtained for the Am-Homogeneous fuel configuration, mainly by the less amount of Am content when blankets are used as well as the lower neutron flux at the edge of the core. Nevertheless, setting blankets in the core caused power peaks at the center of the core, leading to an LHGR of 337 W/cm, which exceeds the maximum allowable LHGR adopted for de ELFR reference core of 330 W/cm. Then, an optimization of the blankets should be performed to reduce the LHGR.

Regarding Am transmutation, in both fuel configurations, a consumption of Am was found, being higher in the Am-Homogeneous fuel configuration due to the higher neutron flux, which allows a better transmutation rate, compared to Am-Heterogeneous fuel configuration. The maximum allowable Am consumption was 8.186 Kg and 1.572 Kg for Am-Homogeneous and Am-Heterogeneous, respectively. A good option to improve the transmutation efficiency especially when Am blankets are used would be to increase the burn-up time as recommended by (NEA, 2014b), passing from 900 to 1800 days, which is the total fuel residence time established for the ELFR reference fuel.

As result of this study, it can be concluded that the best way to consume Am was setting it homogeneously throughout the core, but a transient analysis should be performed to have a better estimation of the reactor behavior under this fuel configuration.

General conclusions

All the objectives defined at the beginning of this doctoral research were successfully achieved. At first, it was possible to create a database about the LFR technology, highlighting the main LFR prototypes that could be studied in future investigations.

The ELFR Serpent model was assessed with the reference data. The neutronic parameters analyzed were close to the expected values, then we can say that the ELFR model was successfully achieved with the Serpent code, taking advantage of its calculation speed up and flexibility.

The use of alternative fuels in the ELFR system was performed with thorium. It was found that the use of ^{232}Th instead of ^{238}U, as fertile material, allows a longer fuel cycle without penalties in the reactor core behavior. In addition, setting the ^{232}Th homogeneously through the core showed the best neutronic performance, with the highest ^{233}U breeding and better power distribution than those found when ^{232}Th blankets were set in the core. In addition, optimization tasks are needed for the use of ThO_2 blankets, in order to reduce the linear heat generation rate and increase the ^{233}U production.

Regarding Am transmutation, as is explained in literature, setting Am nuclides in fuel degrades some neutronic parameters that are important to assure the safety of the core (e.g. Doppler constant, the void worth, the effective delayed neutron fraction). It was observed that setting Am homogeneously caused the highest impact in the neutronic parameters mentioned before, but at the same time, the best Am transmutation rate was achieved under this fuel configuration with suitable power distribution. In addition, the maximum allowable content of Am in the fuel was observed at 7 Wt. % at BoC which is consistent with the literature. On the other hand, even when the impact of Am had a lower impact on the neutronics parameters when Am was set as blankets there were power penalties that could be fixed with a better blankets design, as well as increasing the irradiation time to increase the Am transmutation rate.

As the product of this doctoral research, some papers were written to be published in international journals as well as presented in national and international conferences.

Journal papers:

Luis-Carlos Juárez-Martínez, Juan-Luis François, 2018. Comparative neutronic study of homogeneous and heterogeneous thorium fuel based core design in a lead-cooled fast reactor. Annals of Nuclear Energy, Vol. 114, pp. 102–109.

Luis-Carlos Juárez-Martínez, Juan-Luis François, 2018. Serpent and MCB comparison for neutronics calculations of the European Lead-cooled Fast Reactor. Submitted to Progress in Nuclear Energy (April 2018).

Luis-Carlos Juárez, Juan-Luis François, 2018. Neutronic study of Am transmutation in the ELFR-like model loaded with nitride fuel. Submitted to Annals of Nuclear Energy (May 2018).

Conference papers:

Luis-Carlos Juárez-Martínez, Juan-Luis François, 2017. Análisis de la Inclusión de Torio en el Combustible de un Reactor Rápido Enfriado por Plomo. XXVIII Congreso Anual de la Sociedad Nuclear Mexicana - 2017 LAS/ANS Symposium "New Technologies for a Nuclear Power Expansion Program". Memorias en Formato Digital, CIC CDMX 2017.

Luis-Carlos Juárez-Martínez, Juan-Luis François, 2017. Study on the use of Thorium in a Lead-Cooled Fast Reactor. ANS Winter Meeting & Expo. Transactions of the American Nuclear Society, Vol. 117, Washington, D.C., October 29–November 2, 2017.

Luis-Carlos Juárez-Martínez, Juan-Luis François, 2018. Neutronic Study of Am Transmutation in a Lead-cooled Fast Reactor Loaded with Nitride Fuel. XXIX Congreso Anual de la Sociedad Nuclear Mexicana. Memorias en formato digital, Mérida 2018.

References

1. Abderrahim H.A., Baeten P., Bruyn D., Fernandez R., 2012. MYRRHA – A multi-purpose fast spectrum research reactor. Energy Conversion and Management, Vol. 63, pp. 4-10.
2. Alemberti A., Carlsson J., Malambu E., Orden A., Cinotti L., Struwe D., Agostini P., Monti S., 2011. European lead fast reactor—ELSY. Nuclear Engineering and Design, Vol. 241, pp. 3470-3480.
3. Alemberti A., 2012a. ELFR the European Lead Fast Reactor Design, safety Approach and Safety Characteristics. Technical Meeting on Impact of Fukushima Event on Current and Future Fast Reactor Design. 19-23 March 2012, Dresden Germany.
4. Alemberti A., Carlsson J., Malambu E., Orden A., Cinotti L., Struwe D., 2012b. ELSY-European LFR Activities. Journal of Nuclear Science and Technology, Vol. 48, No. 4, pp. 479-482.
5. Alemberti A., Smirnov V., Smith C.F., Takahashi M., 2013. Overview of lead-cooled fast reactor activities. Progress in Nuclear Energy, Vol. 77, pp. 1-8.
6. Artioli C., Grasso G., Sarotto M., Monti S., Malambu E., 2007. European Leado-cooled SYstem core design: An approach towards sustainability. Sixth Framework Programme EURATOM. Deliverable document.
7. Artioli C., Grasso G., Petrovich C., 2010. A new paradigm for core design aimed at the sustainability of nuclear energy: The solution of the extended equilibrium state. Annals of Nuclear Energy, Vol. 37, pp. 915-922.
8. Aufiero M., Cammi A., Fiorina C., Luzzi L., Sartori A., 2013. A multi-physics time-dependent model for the Lead Fast Reactor single-channel analysis. Nuclear Engineering and Design, Vol. 256, pp. 14-27.
9. Björk K.I., Lau C.W., Nylén H., Sandberg U., 2013. Study of Thorium-Plutonium Fuel for Possible Operating Cycle Extension in PWRs. Science and Technology of Nuclear Installations, Vol. 2013, Number of pages 8.
10. Bortot S., Artioli C., 2011. Investigation of the void reactivity effect in large-size Lead Fast Reactors. Annals of Nuclear Energy, Vol. 38, pp. 1004-1013.
11. Centro Ricerche Bologna (ENEA). Materials specifications. ID: SICNUC-P000-003. Retreived from (2016, August): personal communication with Dr. Giacomo Grasso, Italy.
12. Evalueated Nuclear Data File (ENDF) plotter. Retrieved from: https://www-nds.iaea.org/exfor/endf.htm
13. Evaluated Nuclear Data File (ENDF) plotter. Retrieved from: http://atom.kaeri.re.kr:8080/cgi-bin/endfplot.pl
14. GEN IV International Forum, 2017a. A technology roadmap for generation IV nuclear energy system. Retrieved from (2018, February): https://www.ge4.org/gif/jcms/c_9352/technologyroadmap
15. GEN IV Internatioal Forum, 2017b. Lead-cooled Fast Reactor Technology. Retrieved from (February, 2018): https://www.gen-4.org/gif/jcms/c_9358/lfr
16. Glazov A. G., Leonov V. N., Orlov V. V., Sila-Novitskii A. G., Smirnov V. S., Filin A. I., Tsikunov V. S., 2007. Brest Reactor and Plant-site Nuclear Fuel Cycle. Atomic Energy, Vol. 103, No. 1.

17. Goldberg S.M., Rosner R., 2011. Nuclear Reactors: Generation to Generation. Massachusetts American Academy of Arts and Sciences.
18. Grasso G., Petrovich C., Mattioli D., Artioli C., Sciora P., Gugiu D., G. Bandini., Bubelis E., K Mikityuk, 2014. The core design of ALFRED, a demonstrator for the European lead-cooled reactors. Nuclear Engineering and Design, Vol. 278, pp. 287-301.
19. Grasso G., Petrovich C., Mikityuk K., Mattioli D., Manni F., Gugiu D., 2013a. Demonstrating the Effectiveness of the European LFR Concept: The ALFRED Core Design. Review paper. IAEA-CN-199/312.
20. Grasso G., Alemberti A., Döderlein C., Tuček K., 2013b. Definition of the LFR core and neutronic characterization. LEADER 7th Framework Program. Reference: NRSA/NURAM/13 04 001.
21. György, H., Czifrus Sz., et al., 2017. Investigation on the potential use of thorium as fuel for the Sodium cooled Fast Reactor. Annals of Nuclear Energy, Vol. 103, pp. 238-250.
22. Heuer D., Merle-Lucotte E., Allibert M., Brovchenko M., Ghetta V., Rubiolo P., 2014. Towards the thorium fuel cycle with molten salt fast reactors. Annals of Nuclear Energy, Vol. 64, pp. 421-429.
23. Houas M., Amrani N., Boucenna A., 2016. Evaluation of the Americium transmutation performance in high flux reactors. Annals of Nuclear Energy, Vol. 97, pp. 198-203.
24. Hu W., Jing J., Bi J., Zhao C., Liu B., Ouyang X., 2017. Minor actinides transmutation on pressurized water reactor burnable poison rods. Annals of Nuclear Energy, Vol. 110, pp. 222-229.
25. International Atomic Energy Agency (IAEA), 2005. Thorium fuel cycle – potential benefits and challenges. IAEA-TECDOC-1450, Vienna.
26. International Atomic Energy Agency (IAEA), 2009a. Advanced Reactor Technology Options for Utilization and Transmutation of Actinides in Spent Nuclear Fuel. Austria Vienna.
27. International Atomic Energy Agency (IAEA), 2009b. Status of minor actinide fuel development. IAEA nuclear energy series no. Nf-t-4.6, Vienna.
28. International Atomic Energy Agency (IAEA), 2011. Status and trends of nuclear fuels technology for sodium cooled fast reactors. Nuclear energy series no. NF-T-4.1, Vienna.
29. International Atomic Energy Agency (IAEA), 2012a. Liquid Metal Coolants for Fast Reactors Cooled By Sodium, Lead, and Lead-Bismuth Eutectic. No. NP-T-1.6, Vienna.
30. International Atomic Energy Agency (IAEA), 2012b. Role of Thorium to Supplement Fuel Cycles of Future Nuclear Energy Systems. IAEA Nuclear Energy Series No. NF-T-2.4. Vienna.
31. International Atomic Energy Agency (IAEA), 2016. Climate Change and Nuclear Power. Austria Vienna.
32. International Atomic Energy Agency (IAEA), 2017a. Nuclear Power Reactors in the World. Reference data series No.2, Austria Vienna.
33. International Atomic Energy Agency (IAEA), 2017b. Nuclear Power and Climate Change. Retrieved from (2018, February): https://www.iaea.org/topics/nuclear-power-and-climate-change
34. International Atomic Energy Agency (IAEA), 2018. Depleted Uranium: retrieved from: https://www.iaea.org/topics/spent-fuel-management/depleted-uranium

35. Ivanov N.V., Kazansky Yu.A., Karpovich G.V., 2017. The result of the transmutation of fission fragments in the spectrum of neutrons of thermal and fast reactors. Nuclear Energy and Technology, Vol. 3, pp. 220-223.
36. Jian Z., YiYu C., Hong Y., Yun Hu., 2013. Study of Thorium Utilization in a Large Scale Sodium Cooled Fast Reactor. IAEA-CN-199, Paper CN-199-127, Paris France.
37. Juárez-Martínez L.C., François J.L., 2017. Study on the use of Thorium in a Lead-Cooled Fast Reactor. ANS Winter Meeting & Expo. Washington D.C.
38. Juárez-Martínez L.C., François J.L., 2018. Comparative neutronic study of homogeneous and heterogeneous thorium fuel based core design in a lead-cooled fast reactor. Annals of Nuclear Energy, Vol. 114, pp. 102-109.
39. Kannan U., Krishnani P.D., 2013. Energy from thorium - An Indian perspective. Indian Academy of Sciences, Vol. 38, Part 5, pp. 817-837.
40. Kim Y., Kim W., Kim M., 2014. An international comparative analysis of public acceptance of nuclear energy. Energy Policy, Vol. 66, pp. 475-483.
41. Konings R., Stoller R., Allen T., 2012. Comprehensive Nuclear Materials (Volume 3). European Commission, Joint Research Centre, Institute for Transuranium Elements, Karlsruhe, Germany.
42. Kora K., Nakayaa H., Matsuura H., Goto M., Nakagawa S., Shimakawa S., 2016. A study on transmutation of LLFPs using various types of HTGRs. Nuclear Engineering and Design, Vol. 300, pp. 330-338.
43. Lamarsh J.R., Baratta A., 2001. Introduction to nuclear engineering, third edition, Prentice Hall.
44. Leppänen J., 2007. Development of a New Monte Carlo Reactor Physics Code. Dissertation for the degree of Doctor of Science in Technology. Helsinki University of Technology.
45. Leppänen J., 2009. Serpent progress report. Research report VTT-R-01296-10, *VTT* Technical Research Centre of Finland.
46. Leppänen J., Pusa M., Viitanen T., Valtavirta V., Kaltiaisenaho T., 2015. The Serpent Monte Carlo code: status, development and applications in 2013. Annals of Nuclear Energy, Vol. 82, pp. 142-150.
47. Loewen E.P., Tokuhiro A.T., 2003. Status of Research and Development of the Lead-Alloy-Cooled Fast Reactor. Journal of Nuclear Science and Technology, Vol. 40 No.8, pp. 614-627.
48. Lopez-Soils R.C., François J.L., 2016. Fuel depletion analysis of a small sodium fast reactor with KANEXT and SERPENT, Annals of Nuclear Energy, Vol. 98, pp. 26-35.
49. Marques J.G., 2010. Evolution of nuclear fission reactors: Third generation and beyond. Energy Conversion and Management, Vol. 51, pp. 1774-1780.
50. Matveev V.I., Malysheva I.V., Buriyevskiy I.V., 2015. Physical characteristics of large fast-neutron sodium-cooled reactors with advanced nitride and metallic fuels. Nuclear Energy and Technology, Vol. 1, pp. 308-312.
51. Nuclear Energy Agency (NEA), 2014. State-of-the-art Report on Innovative Fuels for Advanced Nuclear Systems. Organisation for economic co-operation and development (OECD), NEA No. 6895.
52. Nuclear Energy Agency (NEA), 2015a. Perspectives on the Use of Thorium in the Nuclear Fuel Cycle. Extended summary. NEA No. 7228.

53. Nuclear Energy Agency (NEA), 2015b. Introduction of Thorium in the Nuclear Fuel Cycle. Short to long-term considerations. NEA No. 7224.
54. Núñez-Carrera A., Frnacois J.L., Martin Del Campo C., Espinosa-Paredes G., 2008. Feasibility study of boiling water reactor core based on thorium–uranium fuel concept. Energy Conversion and Management, Vol. 49, pp. 47-53.
55. Park T., Lin C.S., Yang W.S., 2016. A moderated target design for minor actinide transmutation in sodium-cooled fast reactor. Annals of Nuclear Energy, Vol. 98, pp. 178-190.
56. Ponomarev A. et al., 2010. Evaluation of Neutron Physics Parameters and Reactivity Coefficients for Sodium Cooled Fast Reactors, Proceedings of ICAPP '10, San Diego, CA, USA, June 13-17, paper 10366.
57. Saito S., 2010. Role of nuclear energy to a future society of shortage of energy resources and global warming. Journal of Nuclear Materials, Vol. 398, pp. 1-9.
58. Serfontein D.E., Mulde E.J., 2014. Thorium-based fuel cycles: Reassessment of fuel economics and proliferation risk. Nuclear Engineering and Design, Vol. 271, pp. 106-113.
59. Shamanin I.V., Grachev V.M., Chertkov Yu.B., Bedenko S.V., Mendoza O., Knyshev V.V., 2018. Neutronic properties of high-temperature gas-cooled reactors with thorium fuel. Annals of Nuclear Energy, Vol. 113, pp. 286-293.
60. Smith C.F., Halsey W.G., Brown N.W., Sienicki J.J., Moisseytsev A., Wade D.C., 2008. SSTAR: The US lead-cooled fast reactor (LFR). Journal of Nuclear Materials, Vol. 376, pp. 255-259.
61. Smith C.F., Cinotti L., 2016. Handbook of Generation IV Nuclear Reactors**.** A volume in Woodhead Publishing Series in Energy, pp.119-155.
62. Stanisz P., Oettingen M., Cetnar J., 2016. Monte Carlo modeling of Lead-Cooled Fast Reactor in adiabatic equilibrium state. Nuclear Engineering and Design, Vol. 301, pp. 341-352.
63. Tesinsky M., Wallenius J., Jolkkonen M., Zhang Y., 2012a. The impact of americium on transients in the European Lead-cooled System ELSY loaded with nitride fuel. Annals of Nuclear Energy, Vol. 50, pp. 56-62.
64. Tesinsky M., 2012b. Science and Technology for Americium Transmutation. Doctoral Thesis, KTH Royal Institute of Technology, Stockholm, Sweden.
65. Toshinskyab Georgy., Petrochenko V., 2012. Modular Lead-Bismuth Fast Reactors in Nuclear Power. Sustainability, Vol. 4, pp. 2293-2316.
66. Toshinskyab G.I., Komlev O.G., Tormyshev I.V., Novikova N.N., Mel´nikov K.G., 2013. Characteristics of Modular Fast Reactor SVBR-100 Using Thorium-Uranium (233) Fuel. IAEA-CN-199/476, Paris France.
67. United Nations (UN), 2017. Aumento de la población mundial. Retrieved from (February, 2018): https://www.un.org/development/desa/es/news/population/world-population-prospects-2017.html
68. Wallenius J., 2012. Physics of americium transmutation. Nuclear engineering and technology, vol.44 no.2, pp. 199-206.
69. Wallenius J., 2013. ELECTRA fuel properties. Version 1.0, Reactor Physics, Stockholm, Sweden.

70. Wojtaszek D., Colton A.V., Bromley B.P., Edwards G.W.R., Levinsky A., 2018. A scenario analysis of once-through thorium fuel cycles with pressure tube HWRs in Canada. Annals of Nuclear Energy, Vol. 111, pp. 152-162.
71. World Nuclear Association (WNA), 2017a. Thorium. Retrieved from (2018, February): http://www.world-nuclear.org/information-library/current-and-future-generation/thorium.aspx
72. World Nuclear Association (WNA), 2017b. Nuclear power in India Retrieved from (2018, February): http://www.world-nuclear.org/information-library/country-profiles/countries-g-n/india.aspx
73. Wu Y., 2016. Design and R&D Progress of China Lead-Based Reactor for ADS Research Facility. Engineering, Vol. 2, pp. 124-131.
74. Yang W. S., Kim Y., Hill R. N., Taiwo T. A., Khalil H. S., 2004. Long-Lived Fission Product Transmutation Studies. NUCLEAR SCIENCE AND ENGINEERING, Vol. 146, pp. 291-318.
75. Yu C., Li X., Cai X., Zou C., Ma Y., Han J., Chen J., 2015. Analysis of minor actinides transmutation for a Molten Salt Fast Reactor. Annals of Nuclear Energy, Vol. 85, pp. 597-604.
76. Zhang Y., 2012. Transmutation of Am in sodium fast reactors and accelerator driven systems. Doctoral Thesis, KTH Royal Institute of Technology, Stockholm Sweden.
77. Zhang Y., Wallenius J., Jolkkonen M., 2013. Transmutation of americium in a large sized sodium-cooled fast reactor loaded with nitride fuel. Annals of Nuclear Energy, Vol. 53, pp. 26-34.
78. Zhang Y., Wallenius J., 2014. Upper limits to americium concentration in large sized sodium-cooled fast reactors loaded with metallic fuel. Annals of Nuclear Energy, Vol. 70, pp. 180-187.